Acta Geophysica (2026) 74:282
https://doi.org/10.1007/s11600-026-02016-x

RESEARCH ARTICLE - HYDROLOGY AND HYDRAULICS

Coupling WRF with HEC-HMS for streamflow forecasting in typical mountainous catchments of northwestern Iran

Sajad Akbari Moghaddam Sani[1] · Mohammad Reza Kavianpour[1] · Mohammad Saeed Najafi[2] · Razieh Noroozian[1]

Received: 13 April 2026 / Accepted: 20 August 2026 / Published online: 9 September 2026
© The Author(s) 2026

Abstract

Nowadays, with the increase in the frequency of extreme rainfall events, the alerts provided by real-time flood forecasting systems are becoming essential to provide accurate and timely information for emergency response. This study uses the Weather Research and Forecasting (WRF) model and the Hydrologic Engineering Center-Hydrologic Modeling System (HEC-HMS) to assess heavy rainfall and runoff forecasting. The models were applied to the upstream basin of Shahid Kazemi Dam, Zarineh-Rood River, located northwest of Iran. The predictability of the WRF model with different microphysics, cumulus (CU), and planetary boundary layer (PBL) parameterizations is evaluated to identify the best set of physics parameters and optimize WRF for forecasting heavy rainfall events. The HEC-HMS model was calibrated by comparing its results with the data observed at gauge stations. The output rainfall data from the top 9 configurations of the WRF model were used as rainfall input in the calibrated HEC-HMS model to investigate the importance of the physical parameterization of the WRF model in runoff forecasting, and the results were examined using statistical indices. Kessler, MYJ, and Grell 3D schemes show the best results for microphysics, CU, and PBL. Consequently, this configuration is recommended for short-term rainfall forecasting tasks in northwest Iran. However, the accurate performance of the WRF model alongside HEC-HMS depends on choosing the best configuration. Still, optimal schemes for precipitation forecasting do not always provide the best estimates for runoff in the basin. The findings of this research could aid in developing a dynamic atmospheric-hydrologic integration system, enhancing flood prediction accuracy across various watersheds and climatic conditions.

Keywords Rainfall-runoff · Physical parameterizations · WRF model · HEC-HMS model · Weather forecasting · Streamflow simulation

Introduction

In recent years, the increasing frequency and intensity of floods worldwide have drawn attention to the critical role of accurate precipitation forecasting in mitigating the adverse impacts of these natural disasters (Ali et al. 2014; Borga et al. 2014; Luo et al. 2018; Tunas et al. 2021). Floods can result in significant financial, individual, and social losses (Hegdahl et al. 2021). The economic burden and hazards associated with rainfall-induced floods are evident, with global flood damage estimated at a staggering $118 billion in 2013 alone, coupled with over 9800 recorded fatalities (Centre for Research on the Epidemiology of Disasters 2014). By providing advance notifications through flood predictions, governing bodies and the general population can implement essential actions to minimize the consequences of floods (Pappenberger et al. 2015). This imperative becomes even more pronounced in the context of the potential worsening

Edited by Dr. Senlin Zhu (ASSOCIATE EDITOR) / Dr. Roger Moussa (CO-EDITOR-IN-CHIEF).

✉ Sajad Akbari Moghaddam Sani
sajad.akbari@doktorant.umk.pl

Mohammad Reza Kavianpour
kavianpour@kntu.ac.ir

Mohammad Saeed Najafi
ms.najafi@wri.ac.ir

Razieh Noroozian
razieh.noroozian@doktorant.umk.pl

[1] Department of Water and Hydraulic Structures, Civil Engineering, K. N. Toosi University of Technology, Tehran, Iran

[2] Department of Water Resources Study and Research (WRR), Water Research Institute (WRI), Tehran, Iran

of heavy rainfall events due to climate change, which has emerged as a significant global concern (Ahern et al. 2005; Hallegatte et al. 2013; Knapp et al. 2008). These figures underscore the necessity of advancing our understanding and management of extreme precipitation events.

To address the challenges posed by increasing flood risks, numerical weather prediction (NWP) models have evolved into indispensable tools, enabling extended flood forecast lead times beyond the response time of watersheds (Rogelis and Werner 2018). Despite the progress made in numerical weather prediction (NWP) systems, accurately simulating and forecasting rainfall remains a formidable challenge. This difficulty stems from the intricate formation mechanisms of rainfall and its significant spatiotemporal variability (Hess and Boers 2022; Tian et al. 2021). The accuracy of NWP rainfall predictions is contingent upon factors such as spatial and temporal resolution and lead time in meteorological models (Jabbari et al. 2019). These predictions, crucial for flood forecasting in hydrological models, are predominantly influenced by the timing, localization, and intensity of events (Habets et al. 2004). The regional climate models (RCM) are the new generation of convection-permitting atmospheric models with a horizontal resolution of 1–4 km; they represent the only NWP models operating at the scale of hydrological catchments prone to flash floods. Their quantitative precipitation forecasts can directly drive rainfall-runoff models, eliminating additional downscaling procedures required for larger-scale NWP systems (e.g., Deidda 2000; Thirel et al. 2010). However, even with these advancements, uncertainties in rainfall location can have detrimental effects on accurate discharge forecasting. Uncertainties in rainfall location can have harmful effects on accurate discharge forecasting. Even a tiny error, such as a 50 km shift, which may be considered minor in meteorological forecasts, can cause the simulation to completely miss a flash flood event if the heaviest predicted rainfalls outside the watershed due to an error in predicting the location of rainfall (Vincendon et al. 2011).

The widely utilized WRF model is pivotal in accurate runoff forecasting at several lead times (Shrestha et al. 2013). The coupled hydrometeorological model has been pivotal in enhancing flood forecasting accuracy and long lead time. Studies such as those by (Chen et al. 2024, T. Zhang et al. 2023, and Zhou et al. 2018) have demonstrated the effectiveness of coupling WRF with hydrological models to simulate precipitation and streamflow variations, optimize parameter schemes, and improve flood forecast capabilities in various river basins and regions. (Chen et al. 2024) showed that the coupling simulation results were better than those of traditional forecast methods, prolonging the flood forecast period. This coupling facilitates a better understanding of atmosphere–land interactions, leading to more reliable predictions of hydrological processes and improved water resource management (Chen et al. 2024; T. Zhang et al. 2023; Zhou et al. 2018). The WRF model, celebrated for its flexibility, efficiency, and advanced numerical options, has extensive application across research centers and global meteorological organizations (Kumar et al. 2016). Recent research has made significant strides in advancing atmospheric and hydrological modeling, particularly in flood forecasting and simulation. Various modeling approaches and parameterization schemes have been explored to enhance precipitation simulations and hydrological predictions.

In California, (Anderson et al. 2002) utilized the MM5 model and Eta model forecasting data to simulate rainfall events, calibrating the Hydrologic Engineering Center-Hydrologic Modeling System (HEC-HMS) for consistent outputs. (Weisman et al. 2008) analyzed 36-h cumulus forecasts using the Weather Research and Forecasting (WRF-ARW) model, emphasizing the significance of land surface, microphysics, resolution, and planetary boundary layer (PBL) schemes in forecasting accuracy.

(Pleim and Gilliam 2009) compared WRF model simulations with MM5 configurations in the USA, highlighting fewer errors in the WRF simulation model with new physics, particularly in summer. (C. Zhang et al. 2011) used the WRF-ARW model to improve the simulation of modified boundary layer (MBL) clouds over the Southeast Pacific, achieving success with the modified Tiedtke scheme. (Roy and Begam 2013) applied HEC-HMS for hydrological forecasting in the Subarnarekha River, East India, obtaining accurate simulations with semi-annual parameter sets.

(Nasiri and Talebi 2020) ranked subbasins in Chenarsukhteh watershed, Iran, based on flood risk criteria using HEC-HMS. (Goodarzi et al. 2022a, b) studied sustainable city development in Borujerd, Iran, under future climate change scenarios, observing significant changes in precipitation amounts. (Tedla et al. 2022) examined the WRF model's rainfall forecasting accuracy in Ethiopia, noting high accuracy for 1–3-day rainfall forecasting periods. (Merino et al. 2022) investigated hourly precipitation for extreme events using the WRF model in Spain, highlighting the importance of rain gauges and hydrometer stations for accurate measurements.

(Vincendon et al. 2009) highlighted unidirectional coupling's use in predicting flood and runoff, while bidirectional coupling considers feedback mechanisms between the atmosphere and the land. (Jasper and Kaufmann 2003) used the Swiss Model (SM) and Canadian Mesoscale Compressible Community model (MC2) to drive the WaSiM-ETH hydrological model in the Southern Alps.

High-resolution precipitation data are crucial for accurately simulating hydrological processes in large watersheds. Studies by (Yu et al. 1999) and (C. A. Lin et al. 2006) demonstrated this need, with MC2 and the Xinanjiang Model showing potential for flood forecasting

research. The WRF model has significantly advanced numerical weather forecasting and is effective in simulating flood events and hydrological processes, as demonstrated by (Flesch and Reuter 2012) and (Tang and Dennis 2014).

Accurate estimation and forecasting of extreme precipitation are fundamental prerequisites for reliable flood modeling. Previous regional studies have highlighted the critical need to evaluate various gridded precipitation datasets and monthly to seasonal climate forecast models to capture the spatiotemporal dynamics of extreme rainfall events across the diverse climatic zones of Iran (Najafi et al. 2026; Najafi and Akbari Moghaddam Sani, 2022). Building upon these broader meteorological and climatological assessments, the accurate simulation of event-based flash floods requires high-resolution coupling of atmospheric and hydrological models.

Event-based rainfall-runoff modeling approaches are increasingly crucial for dissecting the rapid hydrological responses triggered by short-duration, high-intensity storms, as well as understanding the teleconnections between rainfall extremes and potential flooding (Kanji and Das 2026). In alignment with these recent advancements, the broader relevance of coupling WRF-driven atmospheric simulations with hydrologic models extends beyond historical flood analysis; these integrated systems are indispensable for assessing the impacts of climate change and projecting future extreme rainfall scenarios in vulnerable mountainous watersheds.

This study aims to enhance the effectiveness of hydrological models in flow forecasting, particularly in flood-prone areas, to bolster resilience against climate-induced extreme weather events. The research comprises two primary objectives. They are first conducting a sensitivity analysis of the Weather Research and Forecasting (WRF) model's physical parameters for rainfall forecasting within the Zarineh-Rood River basin in Northwest Iran. This analysis aims to understand better the impact of sensitivity analysis on rainfall predictions in a region characterized by diverse climatic and topographic variations. Secondly, the hydrological modeling of the upstream section of the Zarineh-Rood River, situated upstream of the Shahid Kazemi Dam, will be emphasized. The main goal here is to refine the physical parameterization of the WRF model for rainfall forecasting and evaluate the efficacy of different WRF model configurations in predicting flow within this complex and dynamically changing hydrological landscape. By reducing the inherent uncertainty in quantitative rainfall predictions, this study encompasses a meticulous examination of the impacts of different microphysics, cumulus, and planetary boundary layer schemes on precipitation estimation to identify the most suitable combination of physical parameters in the WRF model for forecasting rainfall and subsequent runoff in the upstream basin of Shahid Kazemi Dam, Zarineh-Rood River, located in the northwest of Iran.

The study area

The study area is situated within the Urmia watershed, located in the northwest of Iran, between the provinces of West Azerbaijan and East Azerbaijan, is located between 45°47′ and 47°20′ longitude and 35°41′ and 37°27′ latitude Fig. 1. This region holds significant ecological importance due to Urmia Lake, Iran's largest lake and the largest saltwater lake in the Middle East (Akbari et al. 2019; Eimanifar and Mohebbi 2007). The average altitude of the study area ranges from approximately 1200 to 2700 m above sea level, featuring a diverse topography of plains, valleys, and mountains, which influence local climate patterns and hydrological processes (Jahangir et al. 2023). The Urmia watershed experiences a semi-arid to arid climate characterized by distinct seasonal variations, including hot and dry summers, cold winters, and moderate spring and autumn seasons. Most precipitation occurs during winter, primarily as snowfall in higher elevations, contributing to the annual water supply through snowmelt in spring (Jahangir et al. 2023). The region is prone to flooding, particularly during spring when snowmelt and rainfall increase the flow of rivers and streams feeding into Urmia Lake. The basin, encompassing an extensive area of about 12,000 square kilometers, is home to the primary Zarineh-Rood River, flowing for approximately 300 km. The Zarineh-Rood River, a major tributary of Lake Urmia, originates in the mountainous regions of northwestern Iran and significantly impacts the Urmia catchment (Jahangir et al. 2023). Rapid urbanization and land use changes have altered natural drainage patterns, increasing the risk of flash floods in some areas (Piadeh et al. 2022). Climate change is expected to significantly alter the region's hydrological cycle and exacerbate both flood and drought risks. Recent advanced CMIP6 projections indicate substantial future alterations in precipitation patterns, temperature variables, and overall climate classifications across Iran (Ghazi et al. 2025). Specifically within the Lake Urmia Basin, these shifting climatic parameters are anticipated to increase the frequency and severity of extreme weather events, drastically impacting meteorological anomalies and regional water resources (Ghazi et al. 2023; Hassani et al. 2020). Therefore, accurate flood forecasting and management under these changing atmospheric conditions are crucial for mitigating the impacts of extreme events and protecting the vulnerable environment and communities in the Urmia watershed.

In the hydrological modeling section of this study, all rainfall and synoptic stations depicted in the study area map Fig. 1 were actively utilized to determine the spatial

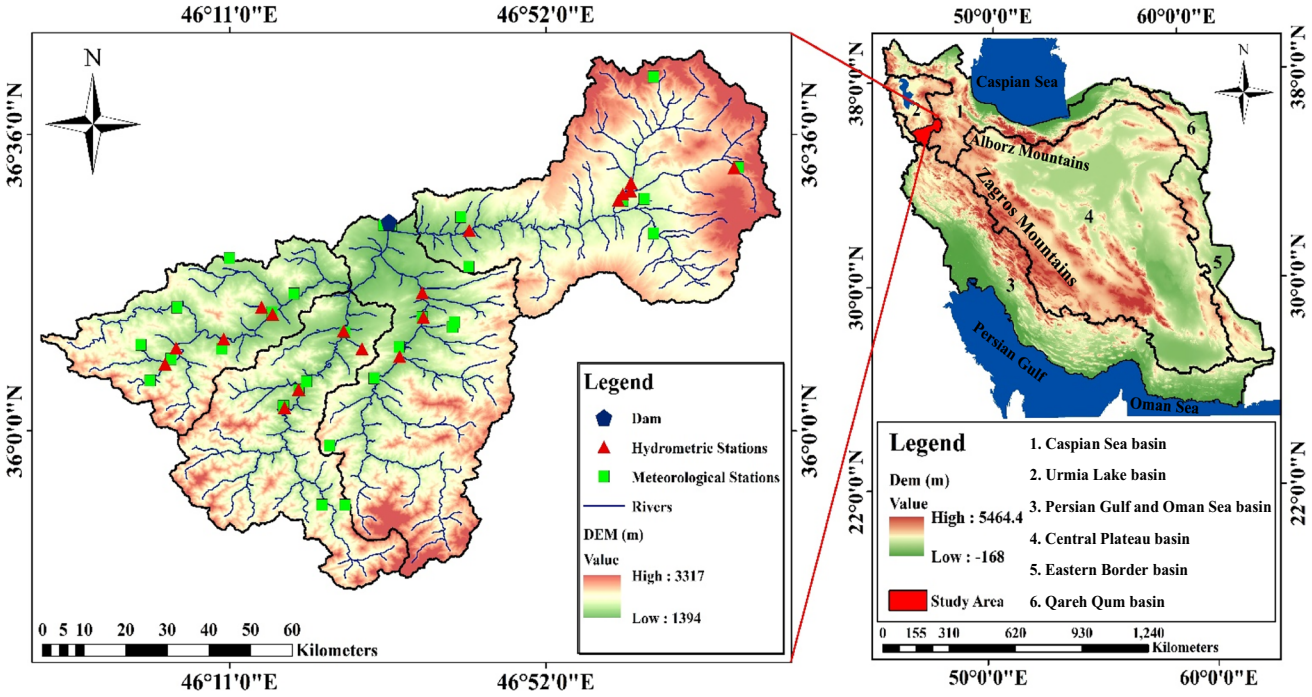


Fig. 1 Geographical and station locations in the study area

distribution of precipitation across the watershed using a weighted scoring approach. To ensure the physical accuracy of the runoff simulations, a rigorous multi-site calibration strategy was implemented in HEC-HMS. Initially, the model was parameterized at the subbasin scale. Observed flow data from local hydrometric stations situated at the downstream end of each of the four individual subbasins were used to calibrate their specific hydrologic responses independently. This localized step ensured that the spatial heterogeneity of the runoff generation was captured. Ultimately, the daily observation data from the Shahid Kazemi Dam, representing the main outlet of the entire watershed, were employed for the final overall calibration and validation of the integrated model across the four selected flood events from 2015 to 2018.

The hydrologic response behavior of the Zarineh-Rood watershed is fundamentally governed by its basin topography, complex drainage network characteristics, and underlying morphometric properties. Recent advanced literature emphasizes that the hydro-geomorphologic and morpho-tectonic characteristics of a watershed significantly dictate runoff generation processes, flow routing efficiency, and overall flood potentiality, particularly in ungauged or topographically complex subbasins (Das and Das 2024; Kanji and Das, 2026). In this mountainous basin, the steep elevation gradients and specific drainage configurations substantially accelerate the time of concentration. This morpho-tectonic nature directly translates high-intensity precipitation events into rapid, short-duration flood peaks, making the accurate simulation of surface runoff highly sensitive to the physical parameterization of the basin.

Data and methodology

Data

This study relies on two distinct datasets, including initial and boundary conditions and observational data concerning rainfall and runoff. These datasets are pivotal for validating and calibrating the models employed in our research. Below, we provide a detailed description of each dataset utilized in this study:

Initial and boundary conditions data

For the atmospheric simulations, the National Centers for Environmental Prediction (NCEP) FNL Operational Model Global Tropospheric Analyses data at a spatial resolution of $1° \times 1°$ were utilized to establish the initial and boundary conditions. To mitigate initialization shocks and allow the model's atmospheric dynamics and moisture convergence fields to stabilize, a spin-up period was applied. Because the target precipitation simulation window for the events was 24 h, a corresponding 24-h spin-up period was implemented prior to the start of each event. The WRF model outputs

generated during this initial adaptation period were strictly discarded and were not used to drive the subsequent HEC-HMS hydrological simulations.

Meteorological observation data

The observational data of rainfall play a pivotal role in our study. This study primarily focused on utilizing 24-h rainfall data to assess the performance and sensitivity of the model to physical parameterization. Data comprising 15 daily precipitation events (Table 1 were collected over a ten-year statistical period spanning from 2008 to 2017. These observations were sourced from a network of six distinct synoptic, rain gauge, and hydrometric sites situated within and adjacent to the study area (Fig. 1). This dataset was crucial for extracting information related to precipitation events. It is worth noting that the available precipitation data vary for each event, resulting in a variable number of stations contributing data for each specific event. We selected four flood events (Table 4 in 2014, 2015, and 2016 for detailed analysis. These events were simulated using the best configurations derived from the WRF model's sensitivity measurements for the Zarineh-Rood basin. Furthermore, we conducted rainfall-runoff modeling for this basin using the forecasted rainfall with the WRF model.

Streamflow reference simulations

In the hydrological modeling section of this study, we have utilized daily observation data from hydrometric stations (Fig. 1). These data cover four flood events occurring from 2015 to 2018, and they serve as a critical component in calibrating the hydrological model. Furthermore, these observations are used to compare the flow predicted by the model, enhancing our understanding of the model's performance in predicting discharge levels in response to varying meteorological conditions.

Table 1 Selected 24-h rainfall events

Events	Date	Average rainfall (mm)
Event-1	2008/01/06	5.76
Event-2	2008/02/12	11.80
Event-3	2008/05/02	12
Event-4	2009/04/13	8.77
Event-5	2010/03/19	12.52
Event-6	2011/01/09	5.55
Event-7	2011/10/29	12.40
Event-8	2012/03/17	11.81
Event-9	2013/01/29	15.85
Event-10	2013/11/20	8.23
Event-11	2014/05/24	5.82
Event-12	2014/10/20	24.54
Event-13	2016/12/02	14.56
Event-14	2017/02/17	9.15
Event-15	2017/05/15	10.30

Models

WRF model

The WRF model is a medium-scale numerical weather prediction model designed to address operational forecasting and atmospheric research requirements (Klemp et al. 2001; Skamarock and Klemp 2008). This study uses the WRF Model, version 4.5, for rainfall forecasts. The simulation domain is centered at 37.739°N and 46.733°E (on a Lambert projection), and a two-way interactive nest is utilized with horizontal resolutions of 12 km (96×102 grid points) and 4 km (142 ×118 grid points), which covers all areas of northwestern Iran Fig. 2.

The uncertainty associated with physical parameterization is an essential source of uncertainty in NWP models (Jansson et al. 2021). It significantly impacts the accuracy of precipitation simulations (e.g., planetary boundary layer, cloud microphysics, short-wave radiation, long-wave radiation, cumulus, etc.). However, planetary boundary layer, microphysics, and cumulus physics are more critical in improving precipitation simulation (Fernández et al. 2007; Najafi and Kuchak 2024).

This study evaluated 14 microphysics schemes, 8 planetary boundary layer (PBL) schemes, and 7 convection schemes within the Weather Research and Forecasting (WRF) model. To capture these atmospheric dynamics, microphysics schemes govern grid-scale atmospheric moisture, resolving the phase changes and fallout of hydrometeors such as cloud water, rain, snow, and ice. Planetary Boundary Layer (PBL) schemes manage the sub-grid-scale vertical turbulent fluxes of heat, moisture, and momentum in the lower atmosphere, directly influencing surface–atmosphere exchanges. Finally, convection schemes—which are entirely synonymous with cumulus parameterizations—are responsible for approximating the effects of sub-grid-scale deep convective updrafts, downdrafts, and localized cloud formation that cannot be explicitly resolved by the model's grid resolution. For each of the 15 selected events, we conducted 29 model runs, resulting in a total of 435 runs (29 runs per event). These extensive simulations allowed us to explore various combinations of microphysics, PBL, and convection schemes to identify the optimal configurations for improving precipitation prediction accuracy. For the list of schemes used in this study, please refer to Table 2. Therefore, nine different configurations of the best schemes of the

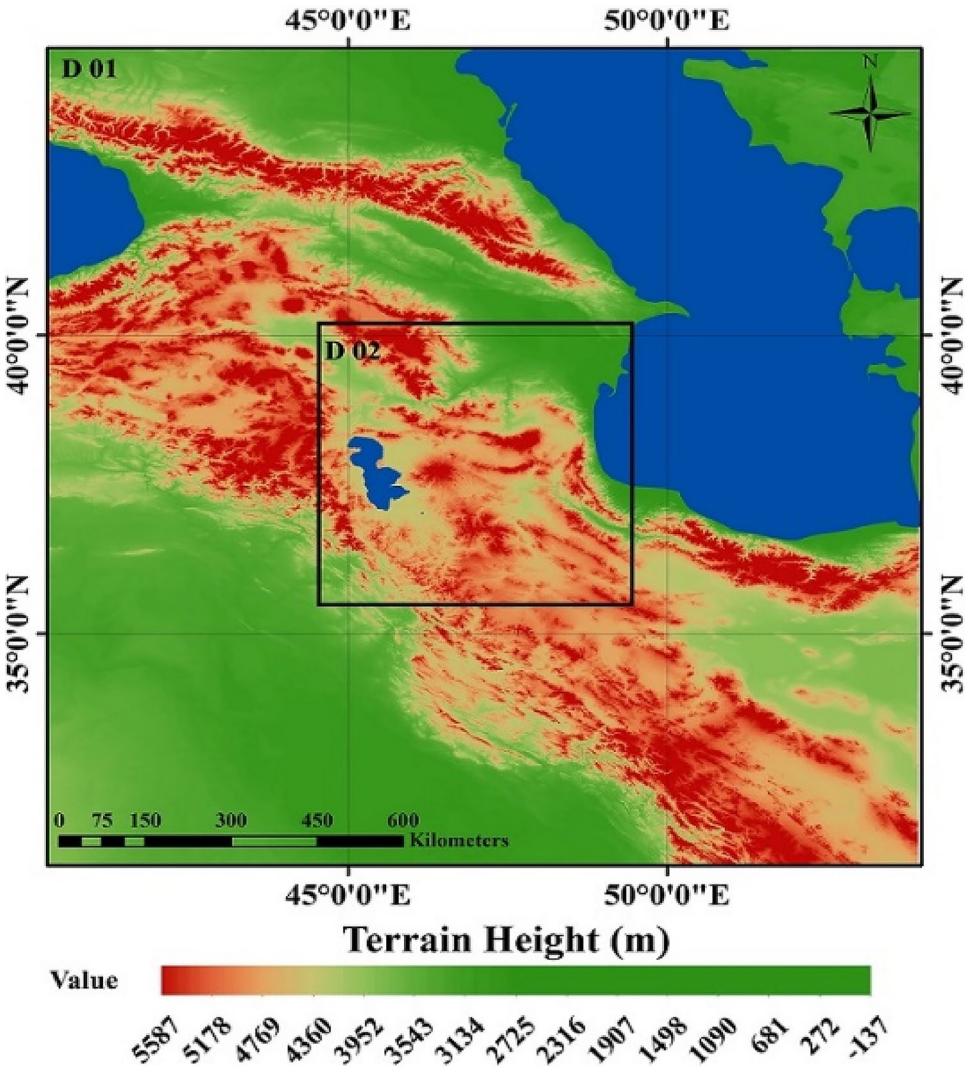


Fig. 2 Model domains (d01 and d02) are used in the WRF model

WRF model were used to reduce this source of uncertainty Table 3.

While short-wave radiation, long-wave radiation, and land surface models (LSMs) play vital roles in continuous, long-term climate simulations, this study isolates microphysics, planetary boundary layer (PBL), and cumulus parameterizations. For short-term, extreme precipitation events, these three physical mechanisms have the most direct, dominant, and immediate impact on convective initiation, moisture convergence, and the structural evolution of heavy rainfall. Consequently, the sensitivity analysis was restricted to these primary drivers to optimize computational efficiency while capturing the core dynamics of flash flood–producing storms.

HEC-HMS model

The Hydrologic Engineering Center's Hydrologic Modeling System (HEC-HMS) is a comprehensive software tool crafted by the U.S. Army Corps of Engineers to facilitate hydrological modeling and watershed runoff simulation. Its utility spans various domains, including but not limited to flood forecasting, reservoir management, and water resource planning. This study employs version 4.10 of the HEC-HMS model (Bartles et al., n.d.), chosen for its enhanced functionality, allowing the importation of grid data.

In this study, a one-way offline coupling approach was utilized to link the WRF atmospheric model with the HEC-HMS hydrological model. Specifically, the precipitation fields forecasted by the WRF model were extracted and fed directly into the calibrated HEC-HMS model as meteorological boundary conditions, without any bidirectional feedback mechanisms from the land surface back to the atmosphere. Integrating various models and methodologies into flood forecasting systems can highlight discrepancies between simulated hydrographs and actual observations (Givati et al. 2016).

Table 2 Summary of the schemes used and the combination of microphysics, PBL, and cumulus physics schemes selected

Microphysics:	
Kessler (Kessler 1969)	MYDM-7 (Milbrandt and Yau 2005)
Lin (Y.-L. Lin et al. 1983)	Morrison (Hong and Pan 1998)
WSM3 (Hong et al. 2004)	CAM5 (Eaton 2011)
WSM5 (Hong et al. 2004)	SUB_YLIN (Y. Lin and Colle 2011)
Eta (Rogers et al. 2001)	WDM5 (Lim and Hong 2010)
WSM6 (Lim and Hong 2010)	WDM6 (Lim and Hong 2010)
Thompson (Thompson et al. 2008)	NSSL (Ziegler 1985)
Short-wave radiation:	
Goddard (Chou and Suarez 1994)	
Dudhia (Dudhia 1989)	
RRTMG (Iacono et al. 2008)	
Long-wave radiation:	
RRTM (Wild et al. 2001)	
PBL:	BouLac (Bougeault and Lacarrere 1989)
YSU (Hong et al. 2004)	UWMT (Bretherton and Park 2009)
MYJ (Janjić, 1994)	Shin-Hong (Shin and Hong 2011)
MYNN2 (Nakanishi and Niino 2004)	GBM (Grenier and Bretherton 2001)
ACM2 (Pleim 2007)	
Surface:	
Revised Monin and Obukhov (Monin and Obukhov 1954)	
Cumulus convection:	Modified Kain–Fritsch
Kain–Fritsch (KF) (Kain 2004)	Multi-scale Kain–Fritsch
Betts–Miller–Janjic (Janjić, 1994)	Arakawa–Schubert (Han and Pan 2011)
Grell 3D Ensemble (Grell and Dévényi 2002)	Tiedtke (Tiedtke 1989)

Table 3 Combinations of best schemes and optimal configurations

Configurations	Microphysics schemes	Planetary boundary layer schemes	Cumulus convection schemes
Config-1	Kessler	MYJ	Grell 3D
Config-2		YSU	Kain–Fritsch
Config-3		BouLac	KF Cumulus Potential
Config-4	CAM	MYJ	Grell 3D
Config-5		YSU	Kain–Fritsch
Config-6		BouLac	KF Cumulus Potential
Config-7	WSM3	MYJ	Grell 3D
Config-8		YSU	Kain–Fritsch
Config-9		BouLac	KF Cumulus Potential

HEC-HMS model components The calculation process within the HEC-HMS model commences from the basin's upper reaches and progressively moves downstream through the various components toward the basin outlet. The model's structure is divided into three primary parts: the basin model, meteorological model, and control parameters, all of which play integral roles in simulating the hydrological response of the watershed to varying meteorological inputs (Soleymani et al. 2006). Various parameters of the catchment, including loss parameters, curve number, transform model, and time of concentration, must be initially entered into the HEC-HMS model to implement it effectively (Custódio and Ghisi 2023).

The physical setup of the basin model in HEC-HMS was established utilizing GIS processing tools. (Table 4) As depicted in the study area map, the Zarineh-Rood watershed was delineated into four primary contributing subbasins (designated as Subbasin 1, Subbasin 2, Subbasin 3, and Subbasin 4, as detailed in Table 5) and their corresponding river reaches using a standard flow accumulation threshold of 1% of the total basin area. This threshold effectively captures the main drainage networks necessary for event-based routing. Furthermore, for the model's control specifications, a computational time step of 24 h (daily) was implemented. This daily interval was selected to align precisely with the temporal resolution of both the aggregated WRF meteorological outputs and the available daily observational discharge data from the Shahid Kazemi Dam hydrometric station.

Loss model: The calculation of runoff volume in loss models revolves around deducting lost water volume from

Table 4 Comparison of observed and simulated peak discharge and total water volume in calibrated model

Events	Date	Observation		Simulation		RMSE Std Dev	NSE	PBias
		Peak flow (m^3/s)	Total volume (MCM)	Peak flow (m^3/s)	Total volume (MCM)			
Event-16	15–21 November 2015	217.3	6.65	219	6.69	0.1	0.99	1.13
Event-17	09–15 April 2015	249.3	13.59	250.1	13.32	0.3	0.91	-3.67
Event-18	10–15 February 2018	241	8.38	243.6	8.89	0.2	0.95	4.61
Event-19	16–21 February 2018	552.5	15.15	544.2	16.34	0.2	0.97	8.93

Table 5 Simulation components of various HEC-HMS model elements for Event-18

Subbasins	Curve number	Impervious area (%)	Initial loss (mm)	Initial discharge (m^3/s)	Lag time (minute)
Subbasin 1	48	4	12	2	1200
Subbasin 2	85	8	2	5	1200
Subbasin 3	69	6	16	5	1500
Subbasin 4	76	2	2	2	900

rainfall. While HEC-HMS offers multiple options for modeling loss, this study opted for the Soil Conservation Service (SCS) curve loss model due to its versatility, quantitative input data requirements, wide range of runoff estimation capabilities, and proven reliability (Askar 2013; Goodarzi et al. 2024; Lal et al. 2017; Soulis 2021; Uwizeyimana et al. 2019). The direct runoff is computed utilizing the following formulas:

$$Q = P - I_a - S \tag{1}$$

$$S = \frac{25400}{\mathrm{CN}} - 254\mathrm{mm} \tag{2}$$

To compute the curve number, parameters such as land use type, soil hydrological group, and moisture class are initially determined using soil type and land use maps of the region developed in GIS. Subsequently, the curve number is derived utilizing respective tables and the weighted averaging method (Goodarzi et al. 2024; Lal et al. 2017).

Transform model: The HEC-HMS model leverages the unit hydrograph model to temporally or spatially distributed rainfall, elucidating the relationship between rainfall excess and direct runoff (Weaver 2003). For this study, the SCS Unit Hydrograph (SCS-UH) method was selected for the transform model due to its established robustness in event-based runoff simulation. Recent comparative assessments (Chatterjee et al. 2014; Das and Das 2024) demonstrate that while advanced geomorphology-based IUH approaches (such as Nash-GIUH) provide detailed and highly accurate runoff routing, they demand high-resolution physical, morphometric, and cross-sectional datasets. Because such extensive data is unavailable for the ungauged upstream subbasins of the semi-arid Urmia watershed, the empirical robustness of the SCS-UH approach remains the most reliable method for estimating peak flows in this data-scarce environment (Vargas Garay et al. 2019). Utilizing a time-area approach, the SCS method formulates a unit hydrograph that captures the watershed's response to a unit depth of excess rainfall. Lag time (TL) is the primary input parameter for this model, which in turn depends on the time of concentration (TC). These two parameters determine the speed at which a watershed reacts to precipitation (Sultan et al. 2022). Additional details regarding the SCS Unit Hydrograph can be explored in (Shatnawi and Ibrahim 2022).

$$S = \frac{1000}{\mathrm{CN}} - 10 \tag{3}$$

$$t_{\mathrm{Lag}} = \frac{L^{0.8} \times (S+1)^{0.7}}{1900 \times A^{0.5}} \tag{4}$$

$$t_c = 1.67 \times t_{\mathrm{Lag}} \tag{5}$$

t_{Lag} represents the lag time in hours while t_c denotes the time of concentration in hours. Additionally, in the equations, L signifies the main channel length in kilometers, A denotes the area in square kilometers, and S represents the central channel slope.

Channel routing: To simulate the movement of the flood wave through the main river reaches connecting the subbasins, the Lag routing method was employed. The upstream basin of the Zarineh-Rood River is predominantly a steep, mountainous catchment. In such high-gradient headwater systems, flood wave propagation is primarily kinematic and translational; physical attenuation due to floodplain storage is entirely negligible. Because complex hydraulic

routing approaches (such as Muskingum–Cunge) require highly detailed, surveyed channel cross sections to calculate volume attenuation, attempting to apply them in data-scarce regions often introduces artificial numerical errors. Therefore, the Lag method is not merely suitable but physically appropriate for this steep catchment. By simply translating the hydrograph based on reach length and high-gradient flow velocity, it effectively captures the timing of the runoff response without relying on unverified channel geometries.

Error indices

To assess the performance of each scheme within the WRF model, we compare the 24-h predicted precipitation values with the corresponding observational statistics in each region. This evaluation employs various statistical indicators (Eqs. 6–11), including Kling–Gupta Efficiency (KGE), coefficient of determination (R^2), and Root Mean Square Error (RMSE). KGE was specifically selected for precipitation evaluation because it provides a comprehensive assessment by simultaneously balancing correlation, bias, and variability, while RMSE effectively penalizes large errors in rainfall intensity.

Furthermore, evaluating the predictive capacity of the coupled model is crucial for appraising streamflow performance. To evaluate the performance of the HEC-HMS model, we employ the Nash–Sutcliffe Efficiency criterion (NSE), Percent Bias (PBias), and RMSE (Eqs. 11–13). This specific combination was chosen for its applicability to flood events. NSE is heavily influenced by squared differences, making it highly sensitive to peak flow magnitudes and ideal for simulating extreme, short-duration flood events rather than low flows. PBias is incorporated alongside NSE to capture discrepancies in the total runoff volume, ensuring that the overall water mass balance is maintained between the simulated and observed hydrographs.

$$\mathrm{KGE} = 1 - \sqrt{(r-1)^2 + (\propto -1)^2 + (\beta - 1)^2} \tag{6}$$

$$\alpha = \frac{\sigma_s}{\sigma_o} \tag{7}$$

$$\beta = \frac{\mu_s}{\mu_o} \tag{8}$$

In the equations above, μ_s and μ_o denote the respective means of simulated and observed data, while r (Eq. 9) represents the Pearson correlation coefficient. Additionally, σ_s and σ_o correspond to the standard deviations of simulated and observed data, respectively.

$$r = \frac{\sum_{i=1}^{n}(O_i - \overline{O})(P_i - \overline{P})}{\sqrt{\sum_{i=1}^{n}(O_i - \overline{O})^2}\sqrt{\sum_{i=1}^{n}(P_i - \overline{P})^2}} \tag{9}$$

$$R^2 = 1 - \frac{\sum_{i=1}^{n}(O_i - P_i)^2}{\sum_{i=1}^{n}(O_i - \overline{O})^2} \tag{10}$$

$$\mathrm{RMSE} = \sqrt{\frac{\sum_{i=1}^{n}(O_i - P_i)^2}{\mathrm{n}}} \tag{11}$$

$$\mathrm{NSE} = \frac{\sum_{i=1}^{n}(O_i - \overline{O})^2 - \sum_{i=1}^{n}(P_i - O_i)^2}{\sum_{i=1}^{n}(O_i - \overline{O})^2} \tag{12}$$

$$\mathrm{PBIAS} = \sqrt{\frac{\sum_{i=1}^{n}(O_i - P_i) \times 100}{\sum_{i=1}^{n} O_i}} \tag{13}$$

In the equations above, P_i represents the predicted precipitation, O_i is the observed precipitation at meteorological stations, $\overline{O}$ is the mean of observed values, $\overline{P}$ is the mean of predicted values, and n is the number of data points.

Following the evaluation based on the above indices and statistical indicators, the top-performing schemes for each event related to microphysics, planetary boundary layer, and convection (first, second, and third, respectively) will be determined. The frequency of each scheme achieving a top rank is then calculated. Considering the importance of these rankings, each frequency was aggregated using a weighted scoring system, assigning 3 points to rank 1, 2 points to rank 2, and 1 point to rank 3. Finally, the schemes with the highest total weighted score are selected as the best schemes. The overall research methodology of this study is presented as a simplified flowchart in Fig. 3.

Results and discussion

Sensitivity measurement of the WRF model

In this section, the outcomes of the WRF model implementation within the northwestern region of Iran are detailed, with a focus on its sensitivity to variations in microphysics, Planetary Boundary Layer, and Cumulus schemes. The investigation encompasses 15 precipitation events, where the model's performance is evaluated in conjunction with 14 microphysics schemes, 8 planetary boundary layer schemes, and 7 cumulus schemes.

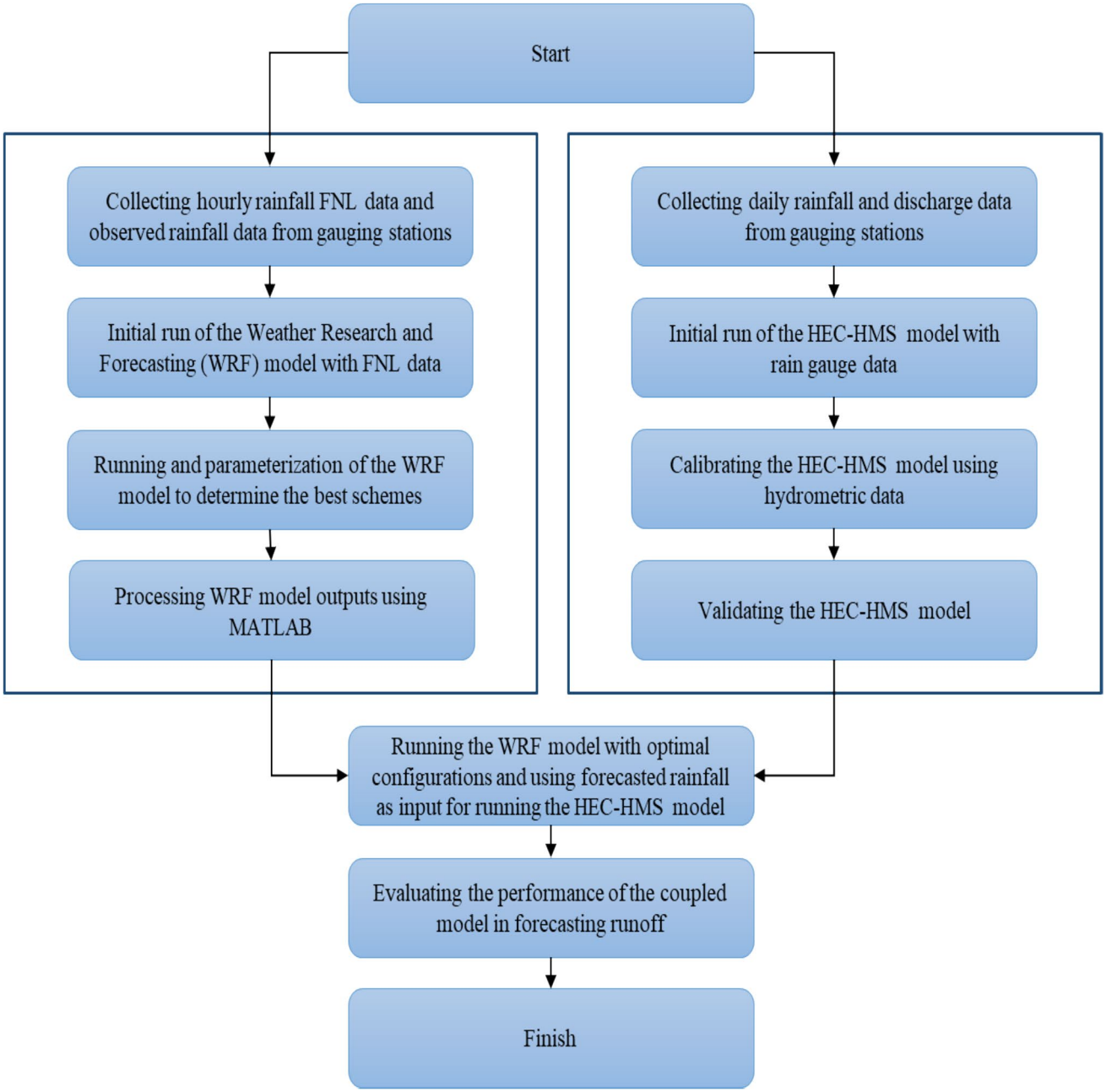


Fig. 3 Research method flowchart

Microphysics parameterization

To assess the impact of different microphysics schemes on rainfall estimation, a comprehensive evaluation was conducted utilizing statistical measures such as Coefficient of Determination (R^2), Kling–Gupta Efficiency (KGE), Root Mean Square Error (RMSE). The examination focused on the Zarineh-Rood River basin and neighboring stations. It is noteworthy that, during the sensitivity analysis, parameters related to convection, planetary boundary layer, short- and long-wave radiation, and surface layer were held constant, with only the microphysics scheme being altered in each implementation.

Figure 4 illustrates the sensitivity of the WRF model to different microphysics parameterizations using RMSE, KGE, and R^2 as performance metrics. Each metric is presented on a color-coded heat map, with shades ranging from dark blue to light blue. For KGE and R^2, darker shades indicate better performance, while for RMSE,

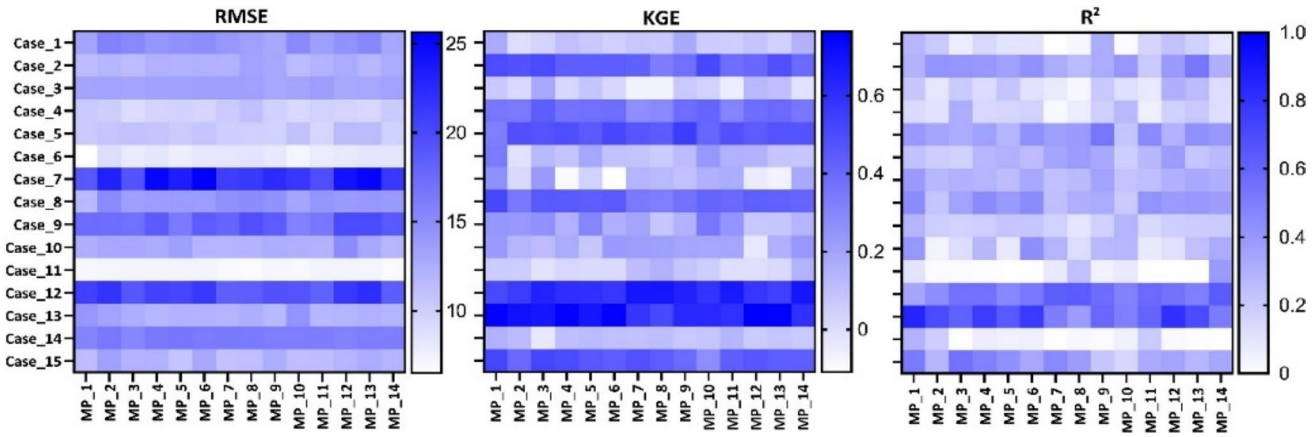


Fig. 4 Heat map of statistical analysis of WRF model with 14 microphysics schemes on 15 rainfall events

lighter shades represent improved accuracy. This color scheme is consistent across Figs. 4, 7, and 10.

The variation in color across different events reflects the model's varying sensitivity to microphysics schemes. Notably, for events 15, 13, 12, 5, and 2, the high KGE and R^2 values suggest that the model performs more efficiently in simulating these events compared to others. Additionally, the differences in the validation indices across microphysics schemes for each event highlight the significant role that microphysics plays in determining the accuracy of precipitation forecasts. It can be noticed that, in general, MP_1 has the highest accuracy on simulation of precipitation, followed by scheme MP_10.

The performance variations among the microphysics schemes highlight their distinct handling of atmospheric moisture and cloud processes over complex terrain. Simpler warm-rain schemes, such as Kessler, performed efficiently in capturing the general precipitation structure in this region without overestimating localized convection. Conversely, more complex mixed-phase ice schemes, like WSM3, showed different sensitivities, frequently overestimating specific humidity convergence and hydrometeor production over the steep topography. This physical dynamic directly impacted the spatial distribution and intensity of the simulated rainfall, propagating substantial volume and timing variations into the subsequent HEC-HMS hydrological modeling.

The sensitivity analysis of the WRF numerical model to microphysics parameterization, incorporating the results from Figs. 5 and 6, revealed a clear hierarchy among the

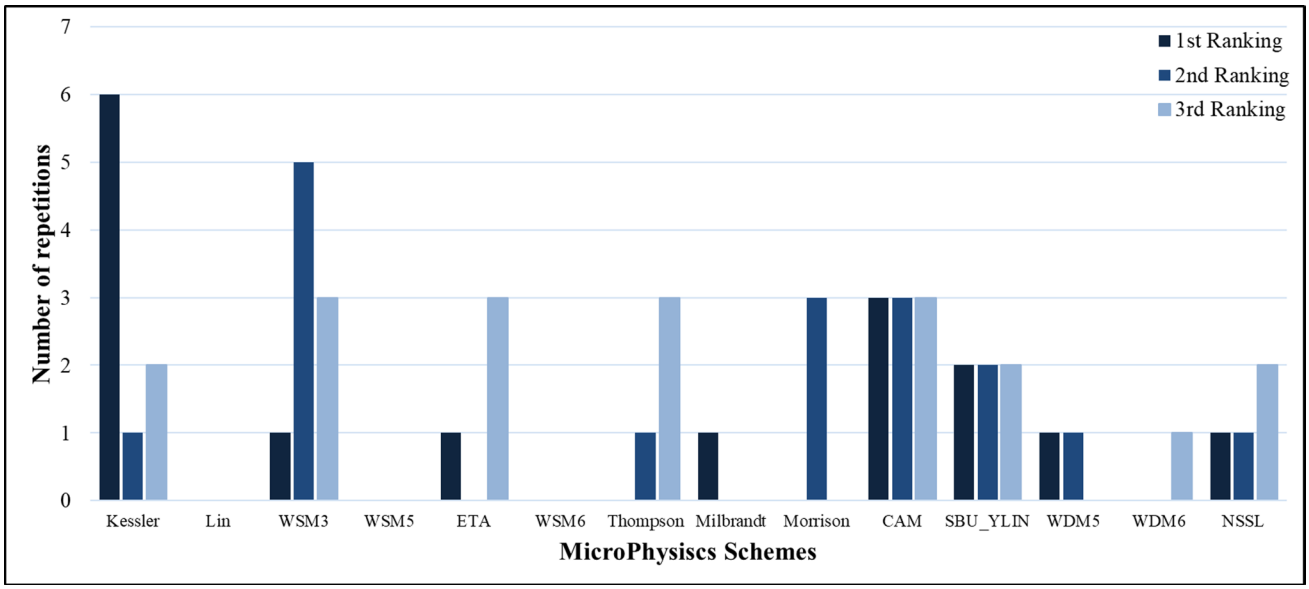


Fig. 5 Effectiveness of microphysical schemes: distribution of ranks 1 to 3 in 15 studied events

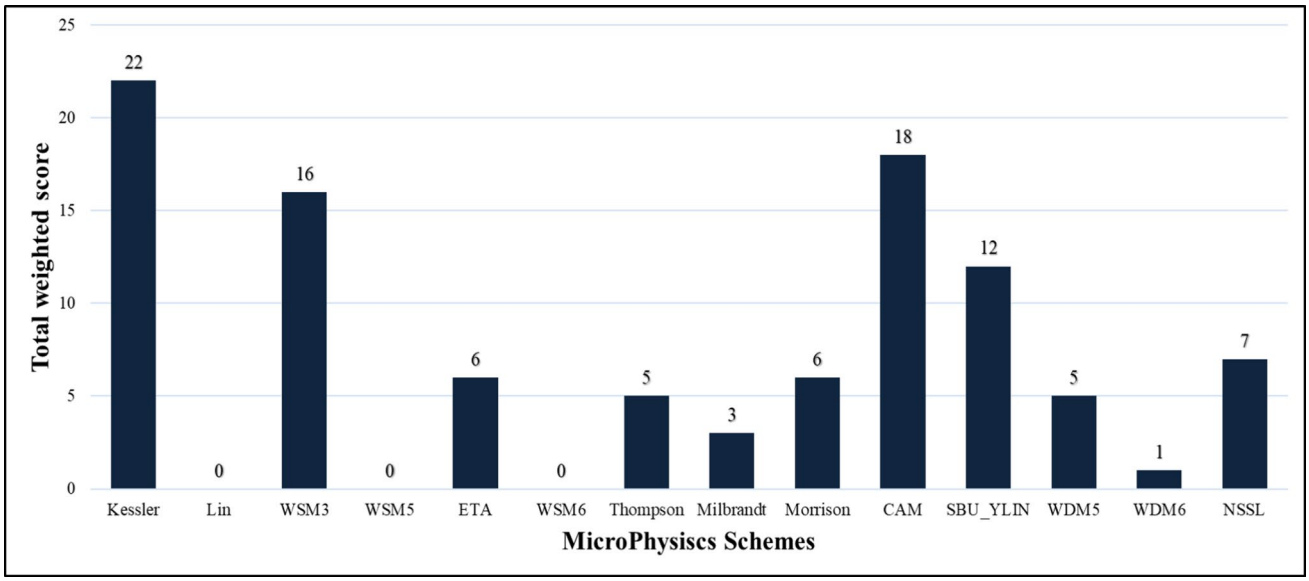


Fig. 6 Efficiency calculation of microphysical schemes using weighted scores

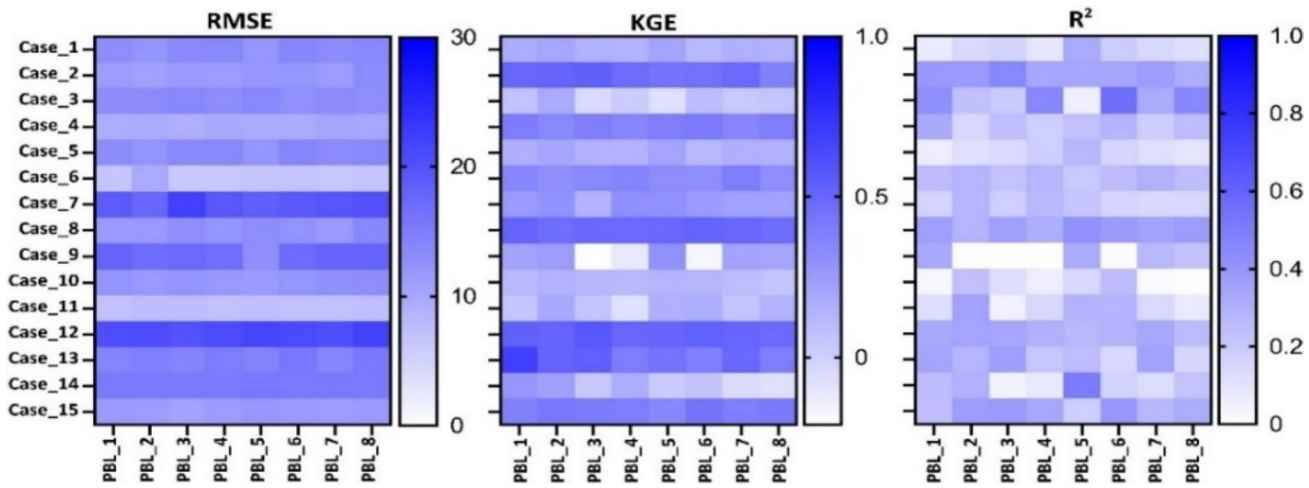


Fig. 7 Heat map of statistical analysis of WRF model with 8 planetary boundary layer schemes on 15 rainfall events

14 investigated schemes across 15 precipitation events in the Zarineh-Rood River basin. The process for selecting the best microphysics schemes involved evaluating validation profiles obtained for each scheme in every event. From this evaluation, the top three schemes were identified for each event. Specifically, the Kessler scheme emerged as the best performer, ranking first in six occurrences, second in one occurrence, and third in two occurrences of precipitation simulation Fig. 5. To quantify the performance of each scheme, a weighted scoring system was applied, assigning coefficients of 3, 2, and 1 to the first, second, and third ranks, respectively. The total weighted score for each scheme was calculated by summing these values across all events. For the Kessler scheme, this resulted in a total weighted score of 22 points, establishing it as the highest scoring and most optimal choice for predicting rainfall in the study area. Following closely were the CAM and WSM3 schemes, which garnered weighted scores of 18–16, respectively, indicating their commendable performance in precipitation estimation within the studied basin Figs. 5 and 6.

This analysis underscores the critical role of selecting appropriate microphysics schemes to enhance the accuracy of rainfall predictions. The results from this section were then integrated into the hydrological model, where the precipitation output from the Kessler scheme was utilized as input for hydrological simulations. By incorporating the most accurate rainfall predictions, the hydrological model's performance in simulating flood events was significantly

improved, leading to enhanced accuracy in flood forecasting and better water resource management in the region.

Planetary boundary layer parameterization

In this phase, the sensitivity of precipitation forecasts to variations in planetary boundary layer (PBL) schemes was investigated, utilizing the Kessler microphysics scheme, previously identified as the optimal choice, as the baseline for all simulations. The aim was to evaluate the performance of eight PBL schemes across 15 precipitation events in the Zarineh-Rood River basin while maintaining other key parameters, such as cumulus, radiation, and surface layer, constant. The analysis focused on 24-h precipitation values, with various evaluation indices, including RMSE, KGE, and R^2, used to assess the accuracy of each scheme.

The performance of these PBL schemes is summarized in the heat map Fig. 7, which highlights that the YSU (PBL_1) and MYJ (PBL_2) schemes consistently perform well across multiple events. Specifically, the YSU scheme showed strong performance in terms of RMSE and KGE, making it highly reliable for rainfall prediction in the region. The MYJ scheme demonstrated particularly high KGE and R^2 values in events 2, 7, and 10, solidifying its reputation for accurate precipitation estimation. The BouLac scheme also performed well but exhibited slightly less consistency than MYJ and YSU.

A deeper analysis of the sensitivity results reveals that the BouLac scheme was the best performer in four of the 15 events, with MYJ and MYNN (PBL_3) excelling in three events each. Meanwhile, YSU and ACM2 (PBL_4) secured the top rank in two events, and UWMT (PBL_7) and Shin-Hong (PBL_8) schemes led in just one event each. Among these schemes, the MYJ consistently ranked high in various events, securing second place in four cases and third in four others. With a final weighted score of 21, MYJ emerged as the top PBL scheme for precipitation estimation in the Zarineh-Rood River basin, followed by BouLac and YSU with scores of 18 each, as shown in Figs. 8 and 9. Therefore, the MYJ scheme was selected as the most appropriate choice for integration into the WRF model for further simulations.

Cumulus parameterization

In this phase, the sensitivity of precipitation forecasts to cumulus parameterization was evaluated using seven distinct cumulus schemes. The optimal microphysics (Kessler) and PBL (MYJ) schemes from previous analyses were set as the baseline configurations, and the performance of each cumulus scheme was assessed by holding other parameters constant.

Figure 10 provides a heat map of the performance of these cumulus schemes across 15 rainfall events, where the Grell 3D and Kain–Fritsch (KF) schemes stood out for their low RMSE and high KGE and R^2 values. The Grell 3D scheme consistently delivered fewer prediction errors in cases like 2, 5, and 12, while the Kain–Fritsch scheme excelled in events 3–7, showing strong adaptability across different scenarios. The heat map clearly illustrates the superior performance of these schemes in minimizing errors and enhancing rainfall prediction accuracy.

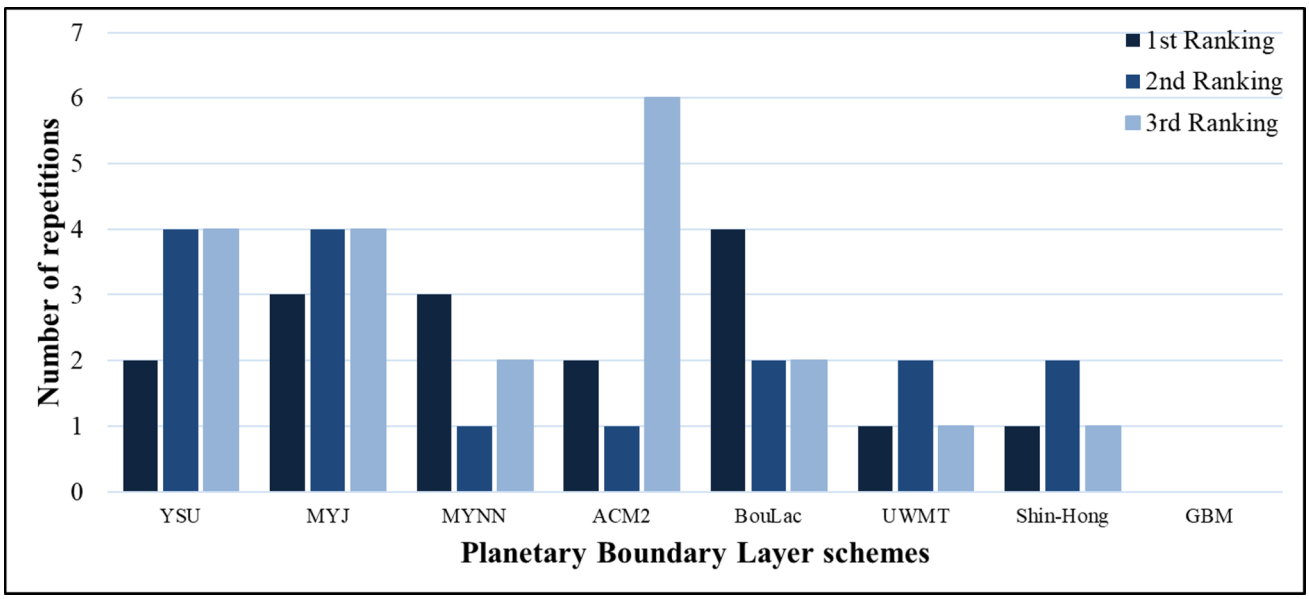


Fig. 8 Effectiveness of PBL schemes: distribution of ranks 1 to 3 in 15 studied events

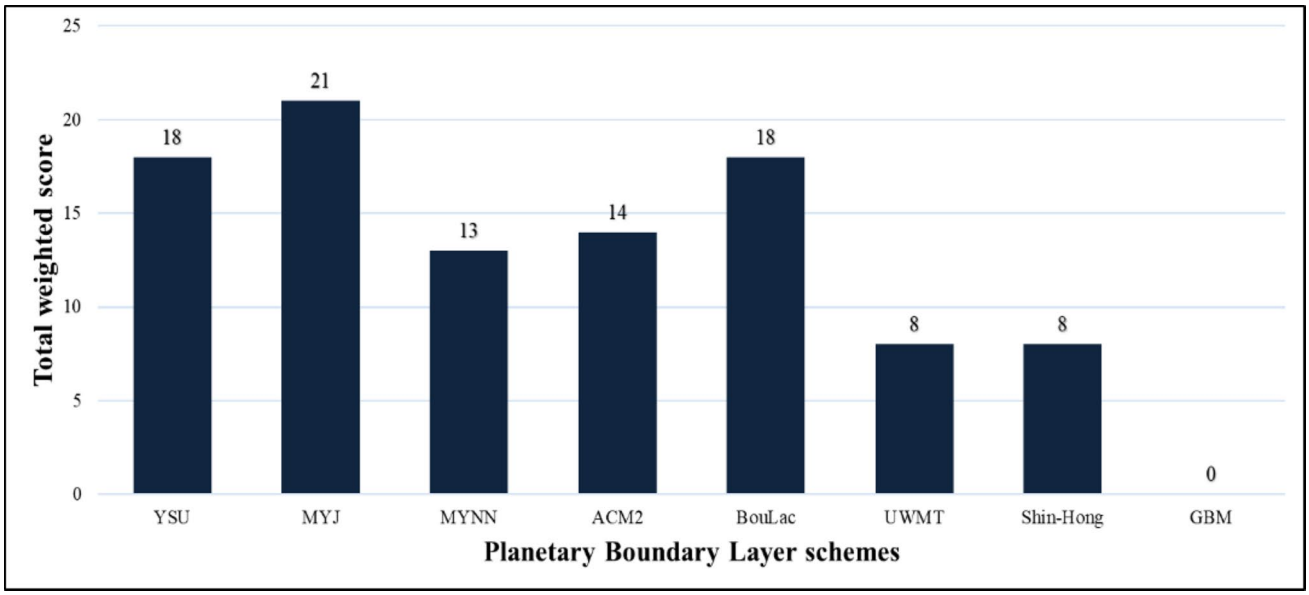


Fig. 9 Efficiency calculation of PBL schemes using weighted scores

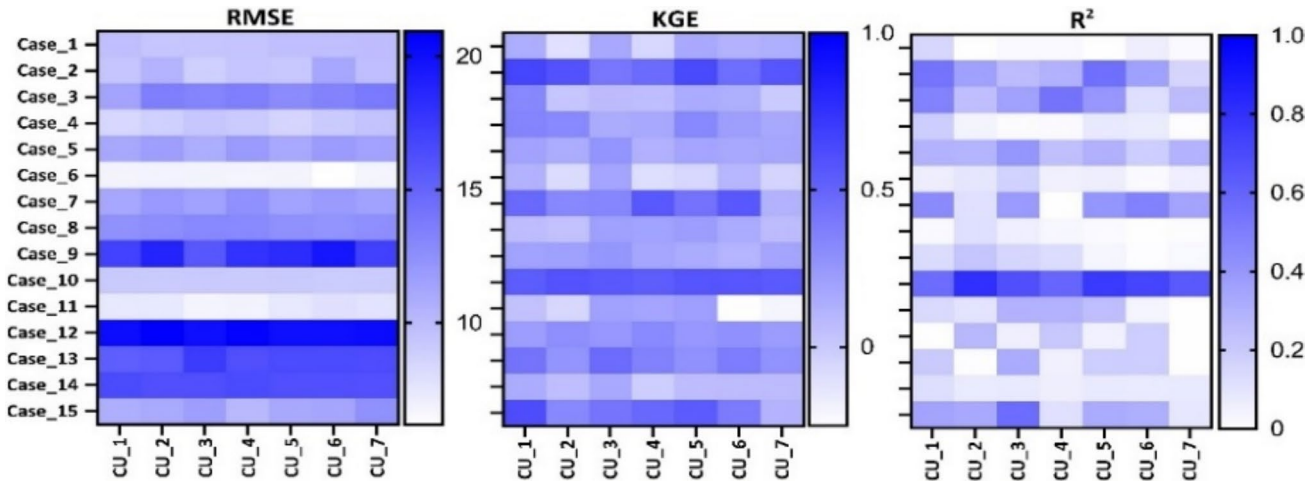


Fig. 10 Heat map of statistical analysis of WRF model with 7 cumulus schemes on 15 rainfall events

Upon further analysis, the Grell 3D scheme emerged as the most effective cumulus parameterization, securing the top rank in seven events, followed by Kain–Fritsch, which ranked first in four events, second in five, and third in three Fig. 11. The Grell 3D scheme achieved a final weighted score of 28, making it the best-performing scheme for precipitation estimation in the Zarineh-Rood River basin. The Kain–Fritsch scheme followed closely with a score of 25, while the KF-CP scheme ranked third with 16 points. Notably, the Arakawa–Schubert scheme failed to secure a top-three ranking in any event, marking it as the least effective for the region, as evidenced by Figs. 11 and 12.

The sensitivity analyses for microphysics, planetary boundary layer (PBL), and cumulus schemes led to the identification of the optimal WRF model configurations for the Zarineh-Rood River basin. Among the microphysics schemes, Kessler, CAM, and WSM3 stood out as the top performers. For PBL schemes, MYJ, YSU, and BouLac showed the best performance, while Grell 3D and Kain–Fritsch emerged as the most effective cumulus schemes for accurate rainfall estimation. The combination of these results provided a foundation for determining the optimal WRF configurations.

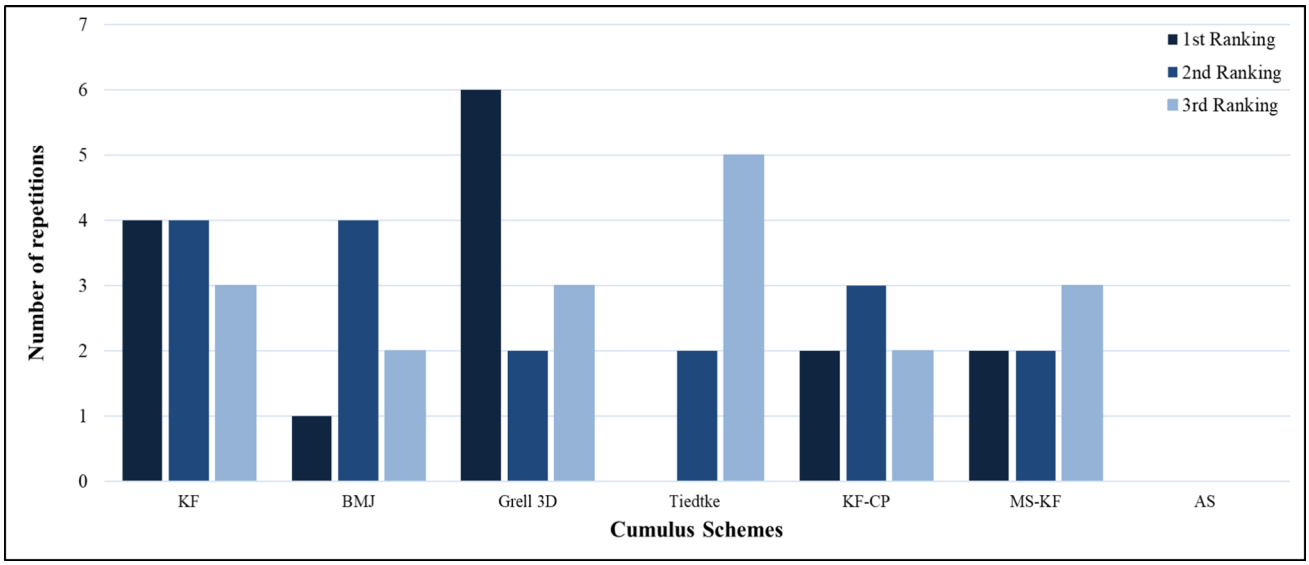


Fig. 11 Effectiveness of cumulus schemes: distribution of ranks 1 to 3 in 15 studied events

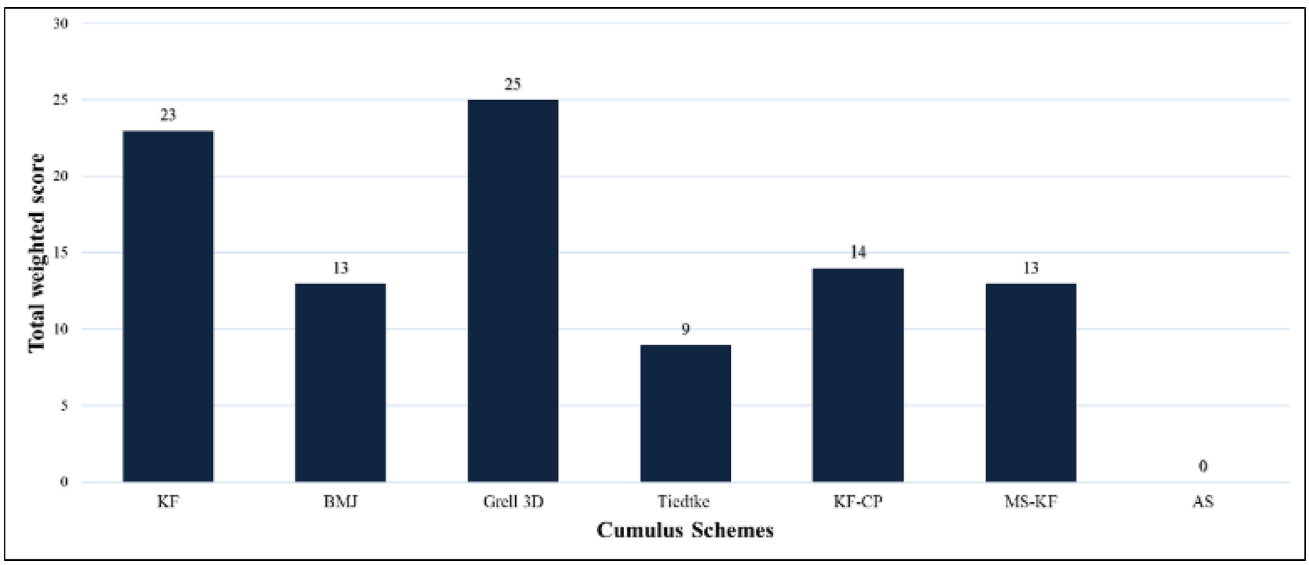


Fig. 12 Efficiency calculation of cumulus schemes using weighted scores

The analysis concluded that the best-performing configuration for rainfall estimation included the Kessler microphysics scheme, MYJ PBL scheme, and Grell 3D cumulus scheme. This combination was applied in subsequent hydrological simulations to enhance the accuracy of rainfall and flood predictions, which were later integrated into streamflow forecasting. To ensure the robustness of the WRF model, nine different combinations of these optimal configurations were tested (detailed in Table 3), with the goal of improving water resource management and flood forecasting in the region.

Rainfall-runoff modeling and HEC-HMS calibration results

In addition to optimizing rainfall forecasts, the study also aimed to assess the sensitivity of the hydrological model to the physical parameters used in the WRF model for discharge simulation. Specifically, the objective was to understand how different configurations of microphysics, PBL, and cumulus schemes influence the accuracy of streamflow simulation in the hydrological model. Nine optimal configurations (Table 3 were developed based on

the best-performing schemes identified in earlier analyses. These configurations were designed to investigate whether combining the best schemes for each parameter results in improved discharge simulation or if alternative combinations yield better overall performance. Furthermore, the analysis explored whether specific interactions among the physical schemes in the WRF model affect predictive efficiency.

To evaluate these configurations, precipitation predictions were conducted for four new 6-day events, with results aggregated over six 24-h intervals. These predictions were then fed into a hydrological model to simulate discharge, focusing on streamflow simulation metrics such as Nash–Sutcliffe Efficiency (NSE), Kling–Gupta Efficiency (KGE), and RMSE. The assessment revealed that configurations combining the Kessler microphysics, MYJ PBL, and Grell 3D cumulus schemes consistently produced accurate streamflow simulations, confirming the robustness of these parameterizations in hydrological applications. However, testing alternative configurations highlighted the importance of considering interactions between different schemes to further enhance model performance for both rainfall prediction and discharge simulation.

Notably, the results demonstrate that optimal WRF schemes for precipitation forecasting do not always provide the best estimates for runoff. This discrepancy is rooted in the highly nonlinear nature of the rainfall-runoff transformation. A meteorological scheme may produce excellent statistical metrics for basin-averaged rainfall but suffer from spatial displacement errors. For example, shifting the heaviest storm core to a neighboring subbasin with a significantly different time of concentration or soil moisture capacity. Conversely, a scheme with slightly lower overall rainfall accuracy might capture the spatiotemporal distribution of the intense storm core more effectively over critical runoff-contributing areas, ultimately resulting in superior streamflow routing and hydrograph shape.

In the rainfall-runoff modeling section, using the HEC-HMS model, four distinct models were developed, each designed to address the unique characteristics of specific hydrological events. These models incorporated varied inputs and initial conditions aimed at exploring the effectiveness of optimal physical parameterization schemes in point forecasts of precipitation. The primary objective was to assess how these forecasts could improve predictions of basin precipitation and streamflow dynamics in hydrological models.

The baseline calibration and validation of the HEC-HMS model were performed for four significant events (Event-16, Event-17, Event-18, and Event-19). It is important to note that this initial calibration was conducted using only observed rain-gauge data. Subsequently, this base-calibrated model was directly forced with the WRF-simulated rainfall inputs (without any further hydrologic recalibration) to evaluate how variations in atmospheric physical parameterizations propagate into the runoff predictions. Table 4 provides a detailed comparison of observed and simulated values for each event, while Fig. 13 illustrates the hydrographs, showing the comparison between modeled and observed streamflow. For Event-16, which occurred from November 15, 2015, to November 21, 2015, the model accurately predicted a peak flow of 219 m^3/s and a total water volume of 6.69 million cubic meters (MCM), closely matching the observed values of 217.3 m^3/s and 6.65 MCM. The high Nash–Sutcliffe Efficiency (NSE) score of 0.99 and minimal Root Mean Square Error (RMSE) confirm the model's high accuracy in simulating this event. Similarly, for Event-17 (April 9 to 15, 2015), the model produced a peak flow prediction of 250.1 m^3/s, which was almost identical to the observed peak of 249.3 m^3/s. The total volume was slightly underestimated (13.32 MCM compared to the observed 13.59 MCM), but the NSE of 0.91 indicates a strong model performance despite the small deviation.

For Event-18, which took place from February 10, 2018, to February 15, 2018, the model slightly overestimated both the peak flow (243.6 m^3/s versus the observed 241 m^3/s) and the total volume (8.89 MCM compared to 8.38 MCM). Nonetheless, the NSE of 0.95 shows that the model maintained its effectiveness in predicting streamflow. Lastly, Event-19, occurring from February 16, 2018, to February 21, 2018, demonstrated a similarly high level of accuracy. The model predicted a peak discharge of 544.2 m^3/s, which was slightly lower than the observed 552.5 m^3/s, while the total water volume was overestimated at 16.34 MCM compared to 15.15 MCM. With an NSE of 0.97, the model proved its reliability in simulating the streamflow for this event as well. These results highlight the robustness of the HEC-HMS model and its ability to predict streamflow dynamics with a high degree of precision, making it a valuable tool in hydrological modeling.

In addition to the HEC-HMS calibration, a detailed assessment of the performance of nine different configurations of the WRF model was conducted for all four selected streamflow events (Event-16 through 19). These configurations were designed to explore the impact of various combinations of microphysics, cumulus, and planetary boundary layer schemes on precipitation and runoff forecasts, as illustrated in Fig. 14. The results showed that Configurations 1 through 6 were highly accurate in predicting both the peak flood discharge and total flood volume. For example, Configurations 1–4 exhibited a near-perfect match between the predicted and observed flows. This accuracy was attributed to the close alignment of the model's initial and boundary conditions (Table 5) such as temperature, soil moisture, and vegetation cover with real-world conditions during the event. The accurate predictions in these configurations underscore

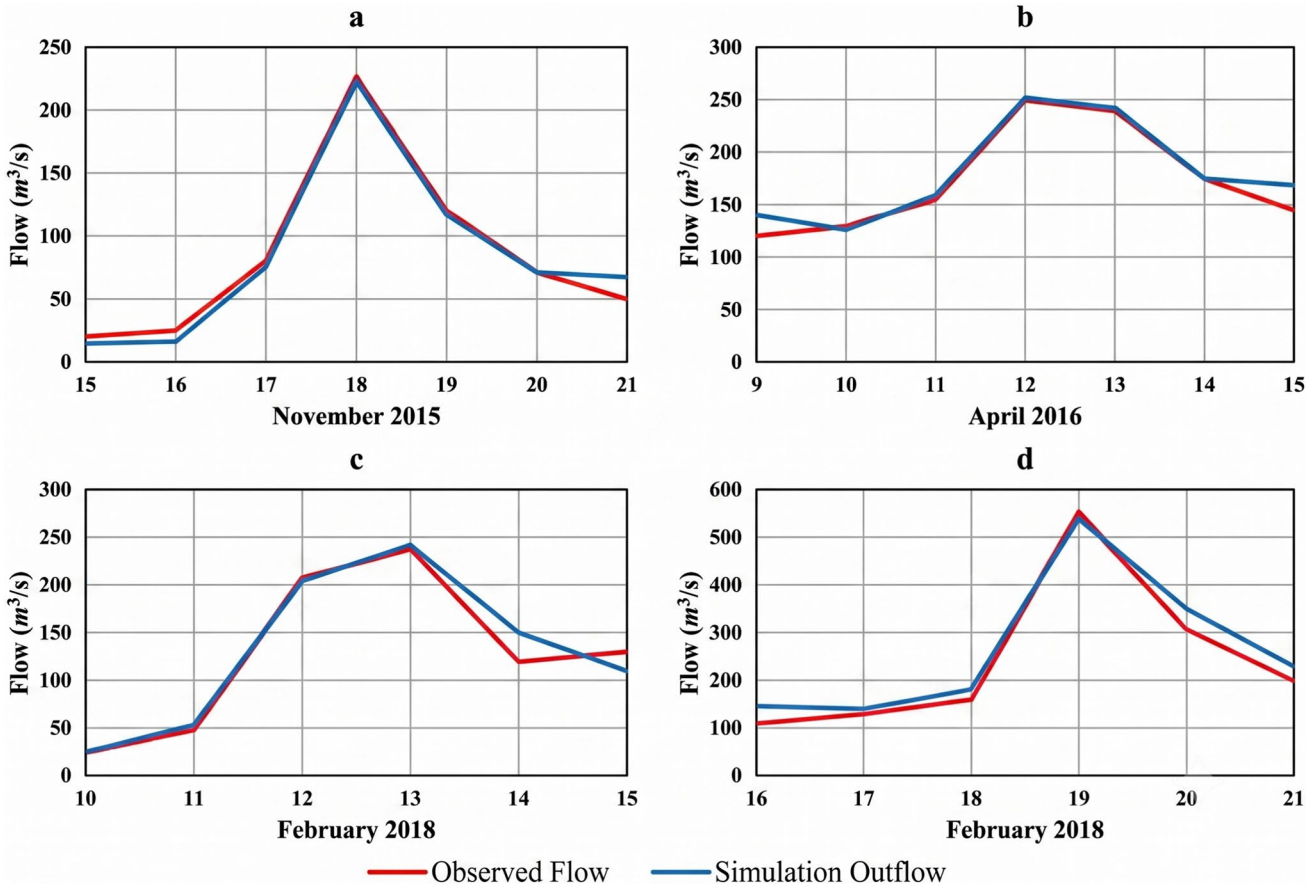


Fig. 13 Calibration outputs: comparison of modeled and observed hydrographs. **a** Event-16, **b** Event-17, **c** Event-18, **d** Event-19

the effectiveness of fine-tuning physical parameterization schemes in improving the model's performance.

The analysis of these configurations illustrates the profound sensitivity of the HEC-HMS model to its meteorological inputs during extreme events, such as Event-18. Different WRF configurations fundamentally alter the spatial distribution and intensity of the simulated rainfall, dictating the subsequent hydrological response. For instance, Configuration 2 under-predicted the flow because its specific combination of physics schemes likely underestimated the localized intensity of the convective storm core over critical runoff-contributing areas, resulting in a subdued streamflow response.

In contrast, Configurations 4 and 7–9 over-predicted the flow. For Configurations 7, 8, and 9, this over-prediction is directly attributed to the WSM3 microphysics scheme. While the WSM3 scheme is highly active and captures overall flow trends well, it frequently generates substantially higher localized rainfall volumes and moisture convergence over this specific complex terrain. Consequently, when these amplified precipitation fields were routed through the HEC-HMS model, they directly translated into over-predicted peak flows at the basin outlet. Despite this overestimation in peak magnitude, the flow patterns and hydrographs for these configurations still closely resembled the timing and shape of the observational model. This confirms that while the choice of microphysics schemes (like WSM3) dictates the absolute volume of the forecast, the coupled WRF/HEC-HMS framework remains highly versatile and robust when properly calibrated for specific hydrological events.

The outcomes from both the HEC-HMS calibration and the WRF model configurations emphasize the critical role that optimal physical parameterization plays in hydrological modeling. By incorporating finely tuned microphysics, cumulus, and planetary boundary layer schemes, the models significantly improved the accuracy of precipitation forecasts, which, in turn, enhanced streamflow predictions. The results presented in Tables 6, 7, 8 and 9 provide a comprehensive comparison of peak discharge and total flood volume for each event, demonstrating a high level of alignment between the observed and simulated values across the various configurations. Evaluation indices, including the NSE and PBias, consistently reflect the success of the recalibrated models in accurately predicting hydrological outcomes.

Integration of optimal physical parameterization schemes in both meteorological and hydrological models

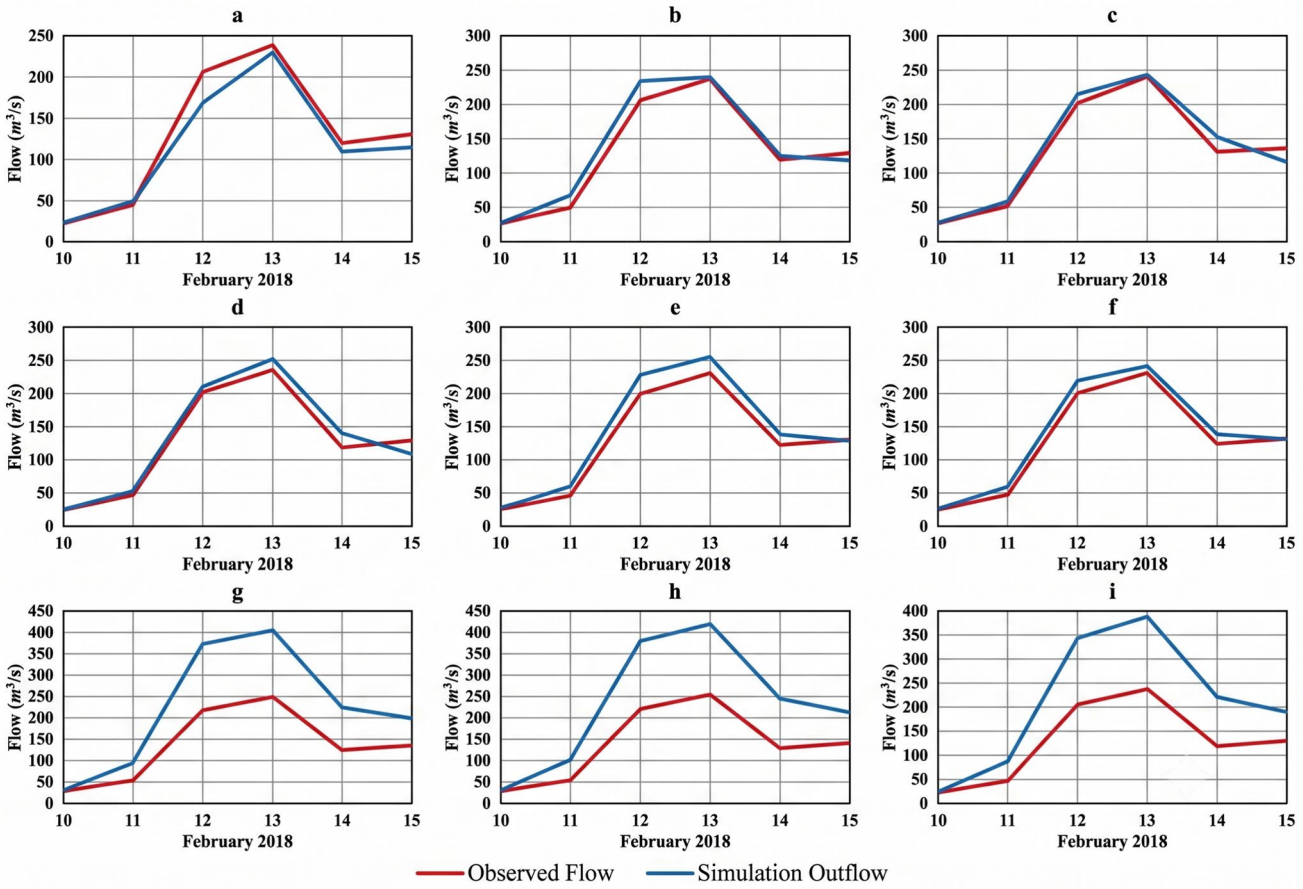


Fig. 14 Performance of 9 configurations in predicting flow for Event-18. **a** Config-1, **b** Config-2, **c** Config-3, **d** Config-4, **e** Config-5, **f** Config-6, **g** Config-7, **h** Config-8, **i** Config-9

Table 6 Predicted vs. Observed peak discharge and flood volume with evaluation indicators for HEC-HMS Rainfall-runoff model–event 16

Configurations	Observation		Simulation		RMSE Std Dev	NSE	PBias
	Peak flow (m^3/s)	Total volume (MCM)	Peak flow (m^3/s)	Total volume (MCM)			
Config. 1	217.3	6.65	173.3	6.37	0.3	0.919	−4
Config. 2	217.3	6.65	141.6	5.28	0.5	0.782	−20.45
Config. 3	217.3	6.65	153.4	5.89	0.4	0.853	−11
Config. 4	217.3	6.65	231.9	8.74	0.5	0.919	31.37
Config. 5	217.3	6.65	223.9	8.12	0.4	0.822	21.52
Config. 6	217.3	6.65	190.1	7.15	0.3	0.914	7.48
Config. 7	217.3	6.65	245	9.12	0.6	0.629	37.21
Config. 8	217.3	6.65	304.5	11.51	1.1	-0.298	73.12
Config. 9	217.3	6.65	332.5	12.3	1.3	-0.725	85.04

has led to superior performance in predicting streamflow dynamics. These advancements in model accuracy offer critical insights for flood management and water resource planning, as they enhance the precision of forecasts in response to extreme weather events.

In Event-16, configurations 1, 3, and 6 demonstrated superior efficiency in predicting flood volume, despite some limitations in estimating the maximum observed discharge of 217.3 m^3/s. Among these, configuration 6 achieved the best flood volume prediction (190.1 m^3/s),

Table 7 Predicted vs. Observed peak discharge and flood volume with evaluation indicators for HEC-HMS Rainfall-runoff model–event 17

Configurations	Observation		Simulation		RMSE Std Dev	NSE	PBias
	Peak flow (m^3/s)	Total volume (MCM)	Peak flow (m^3/s)	Total volume (MCM)			
Config. 1	249.3	13.59	218.7	13.05	0.8	0.397	−5.91
Config. 2	249.3	13.59	278.7	16.10	1	0.083	14.81
Config. 3	249.3	13.59	298.6	16.71	1.1	−0.174	15.85
Config. 4	249.3	13.59	229.6	13.22	0.5	0.756	−4.59
Config. 5	249.3	13.59	240.3	13.75	0.5	0.796	−0.69
Config. 6	249.3	13.59	249.3	13.53	0.3	0.893	−2.2
Config. 7	249.3	13.59	286.3	16.94	1.1	−0.118	22.18
Config. 8	249.3	13.59	294.1	16.18	0.8	0.397	17.3
Config. 9	249.3	13.59	372.3	18.84	1.8	−2.233	34.98

Table 8 Predicted vs. Observed peak discharge and flood volume with evaluation indicators for HEC-HMS Rainfall-runoff model–event 18

Configurations	Observation		Simulation		RMSE Std Dev	NSE	PBias
	Peak flow (m^3/s)	Total volume (MCM)	Peak flow (m^3/s)	Total volume (MCM)			
Config. 1	241	8.38	242.4	9.09	0.2	0.955	6.69
Config. 2	241	8.38	224.4	7.6	0.3	0.924	−10.9
Config. 3	241	8.38	264.9	9.64	0.3	0.923	13.61
Config. 4	241	8.38	253.6	8.84	0.2	0.976	4.17
Config. 5	241	8.38	243	8.26	0.3	0.935	−2.54
Config. 6	241	8.38	246.4	8.48	0.1	0.983	0.1
Config. 7	241	8.38	398.3	14.87	1.4	−1.47	74.89
Config. 8	241	8.38	408.4	14.62	1.4	−0.919	71.72
Config. 9	241	8.38	395	14.17	1.3	−0.639	67.07

Table 9 Predicted vs. Observed peak discharge and flood volume with evaluation indicators for HEC-HMS Rainfall-runoff model–event 19

Configurations	Observation		Simulation		RMSE Std Dev	NSE	PBias
	Peak flow (m^3/s)	Total volume (MCM)	Peak flow (m^3/s)	Total volume (MCM)			
Config. 1	552.5	15.96	458.2	15.84	0.3	0.893	−0.12
Config. 2	552.5	15.96	405	14.18	0.4	0.820	−10.37
Config. 3	552.5	15.96	455.8	15.64	0.3	0.909	−1.12
Config. 4	552.5	15.96	637.8	20.9	0.7	0.550	31.91
Config. 5	552.5	15.96	655.5	21.31	0.7	0.489	34.28
Config. 6	552.5	15.96	541.7	18.05	0.4	0.861	13.93
Config. 7	552.5	15.96	525.1	17.57	0.3	0.891	11.38
Config. 8	552.5	15.96	644.9	20.73	0.6	0.608	30.5
Config. 9	552.5	15.96	597	19.79	0.5	0.706	25.08

while configuration 5 performed the best in peak flow estimation (223.9 m^3/s).

Event-17 presented different dynamics, with configuration 6 again proving most effective in predicting both peak discharge and total flood volume. Configurations 5, 4, and 1 also performed adequately.

In Event-18, configuration 6 exhibited excellent accuracy in predicting peak discharge at 246.4 m^3/s, while

configuration 1 provided an almost exact match for observed values. However, configurations 7–8, featuring different physical parameterizations, significantly overestimated both peak discharge and flood volume.

For Event-19, configuration 1 excelled in predicting flood volume, while configurations 2–3, sharing the Kessler microphysics scheme with configuration 1, also performed well. Surprisingly, configuration 6, which performed admirably in earlier events, showed higher error rates in flood volume estimation, but it excelled in peak discharge prediction (541.7 m^3/s against an observed value of 552.5 m^3/s).

Across all examined events, configurations 1–6 consistently delivered reliable performance, highlighting the importance of combining different physical schemes for effective precipitation and flow forecasting. Among the various physical parameters, the microphysics scheme introduced the most significant variability in both peak discharge and flood volume predictions. Configurations featuring different microphysics schemes, such as Kessler (used in configuration 1) and MYJ (used in configuration 6), exhibited noticeable differences in performance, further underscoring the decisive role of microphysics in the accuracy of flow and hydrological forecasting. Thus, the choice of the microphysics scheme emerges as the most critical factor in achieving accurate model performance.

While this study primarily addresses the meteorological input uncertainties arising from various WRF configurations, it is crucial to acknowledge the inherent uncertainties within the hydrological modeling process itself. A major source of uncertainty stems from the observed discharge data used for HEC-HMS calibration. Streamflow estimates derived from stage-discharge rating curves are particularly prone to extrapolation errors and channel morphological changes during extreme flood events. Recent literature highlights the critical need to account for these observational uncertainties in hydrologic calibration and design flood estimation, often employing advanced frameworks such as Bayesian hydrodynamics (Das and Das 2026). Future modeling efforts in this basin should consider auto-calibration frameworks that explicitly incorporate rating curve uncertainties.

The accurate prediction of hydrological processes is fundamentally dependent on the representation and precision of meteorological forcing, a concept increasingly emphasized by advanced modeling frameworks in contemporary literature. Recent studies have demonstrated that variations and trends in meteorological inputs profoundly influence both short-term flood dynamics and long-term hydrological indices (Dikici and Burgan 2025). Furthermore, the integration of high-resolution meteorological parameters into sophisticated prediction frameworks has been shown to be crucial for capturing complex streamflow dynamics and flood routing accuracy under extreme rainfall conditions (Jam-Jalloh et al. 2024; Mahmoudi et al. 2025). While studies such as Jam-Jalloh et al. (2024) have significantly advanced the field by evaluating how different hydrological model complexities—specifically comparing fully distributed WRF-Hydro systems with semi-distributed HEC-HMS models—affect flood forecasting under a fixed WRF configuration, our study offers a complementary methodological novelty. Specifically, we focus on atmospheric parameterization uncertainty by conducting an exhaustive sensitivity evaluation of 435 distinct WRF physical parameterization combinations. By isolating the effects of microphysics, planetary boundary layer, and cumulus schemes, this study empirically demonstrates a critical nonlinear dynamic: the atmospheric configuration that yields the most statistically accurate basin-averaged rainfall volume does not necessarily produce the most accurate streamflow hydrograph. Because complex terrain severely compounds spatial displacement errors, achieving accurate hydrologic routing requires selecting physical schemes that prioritize the spatiotemporal location of the storm core over absolute total volume accuracy. Our findings directly align with these recent advancements, confirming that the careful selection of atmospheric physics parameterizations, specifically distinguishing between the spatial outputs of warm-rain versus mixed-phase ice schemes, is an absolute prerequisite for reliable streamflow and flood forecasting in topographically complex basins.

Limitations of the study

While this integrated modeling framework demonstrates high predictive capability, certain limitations must be acknowledged. First, the use of a one-way offline coupling approach means that localized land–surface feedbacks—such as the impact of dynamic soil moisture and evapotranspiration changes on atmospheric boundary layer development—are not communicated back to the WRF model during the event. Second, representing a topographically complex mountainous watershed using only six meteorological and hydrometric stations introduces inherent spatial interpolation uncertainties when generating the observed precipitation fields. Finally, the calibration of the HEC-HMS model relies heavily on streamflow estimates derived from stage-discharge rating curves. During the extreme, short-duration flood events analyzed in this study, channel morphology can shift, and rating curves are often extrapolated beyond their measured limits, introducing an unquantified layer of uncertainty into the peak discharge observations against which the models are evaluated.

Conclusion

This comprehensive sensitivity analysis of the Weather Research and Forecasting (WRF) model provides critical insights into the dynamics of precipitation and streamflow

forecasting in Northwestern Iran. The study focused on the microphysics, planetary boundary layer (PBL), and cumulus parameterization schemes, revealing their significant roles in model performance.

The microphysics scheme was identified as a crucial factor, with Kessler, CAM, and WSM3 emerging as the most effective among the 14 investigated schemes. This highlights the importance of selecting the appropriate microphysics scheme, with the Kessler scheme proving particularly efficient in this region. In the PBL category, the MYJ scheme consistently outperformed others in simulating precipitation across various events, making it a key factor in optimizing the WRF model for the study area. Regarding cumulus schemes, the Grell 3D and Kain–Fritsch schemes demonstrated the highest proficiency, especially in low-rainfall scenarios.

When integrated into the HEC-HMS rainfall-runoff model, these parameterizations proved pivotal in accurately predicting flood volumes and peak flows. Configuration 6, which combines the CAM microphysics scheme, BouLac PBL scheme, and the Kain–Fritsch cumulus scheme, was particularly efficient in forecasting flows.

However, the analysis across all events revealed that the microphysics scheme had the most decisive impact on the accuracy of flow and hydrological forecasting. Variations in the microphysics scheme led to the largest discrepancies between predicted and observed values, making it the key factor in determining the precision of the model. Future research should therefore prioritize refining microphysics parameterization to improve model outcomes.

In conclusion, selecting optimal parameterization schemes for microphysics, PBL, and cumulus remains a key factor in enhancing the predictive capability of numerical models, with the microphysics scheme emerging as the most critical element for accurate meteorological and hydrological forecasts in the region.

Authors' contribution All authors contributed to the study conception and design. Material preparation, data collection and analysis were performed by [Sajad Akbari Moghaddam Sani]. Software and visualization performed by [Mohammad Saeed Najafi], [Razieh Noroozian], and [Sajad Akbari Moghaddam Sani]. The first draft of the manuscript was written by [Sajad Akbari Moghaddam Sani] and all authors commented on previous versions of the manuscript. Review and editing performed by [Sajad Akbari Moghaddam Sani] and [Mohammad Saeed Najafi]. Supervision by [Mohammad Reza Kavianpour] and [Mohammad Saeed Najafi]. All authors read and approved the final manuscript.

Funding The authors declare that no funds, grants, or other support were received during the preparation of this manuscript.

Data availability The datasets supporting the findings of this study are available from the corresponding author upon reasonable request. The NCEP GDAS/FNL meteorological datasets are publicly available through the National Centers for Environmental Prediction (NCEP) portals.

Declarations

Conflict of interest The authors have no relevant financial or conflict of interest to disclose.

Open Access This article is licensed under a Creative Commons Attribution 4.0 International License, which permits use, sharing, adaptation, distribution and reproduction in any medium or format, as long as you give appropriate credit to the original author(s) and the source, provide a link to the Creative Commons licence, and indicate if changes were made. The images or other third party material in this article are included in the article's Creative Commons licence, unless indicated otherwise in a credit line to the material. If material is not included in the article's Creative Commons licence and your intended use is not permitted by statutory regulation or exceeds the permitted use, you will need to obtain permission directly from the copyright holder. To view a copy of this licence, visit http://creativecommons.org/licenses/by/4.0/.

References

Ahern M, Kovats RS, Wilkinson P, Few R, Matthies F (2005) Global health impacts of floods: epidemiologic evidence. Epidemiol Rev 27(1):36–46. https://doi.org/10.1093/epirev/mxi004

Akbari M, TorabiHaghighi A, Aghayi MM, Javadian M, Tajrishy M, Kløve B (2019) Assimilation of Satellite-based data for hydrological mapping of precipitation and direct runoff coefficient for the Lake Urmia Basin in Iran. Water 11(8):1624. https://doi.org/10.3390/w11081624

Ali H, Mishra V, Pai DS (2014) Observed and projected urban extreme rainfall events in India. J Geophys Res: Atmos 119(22):12–621. https://doi.org/10.1002/2014JD022264

Anderson ML, Chen Z-Q, Kavvas ML, Feldman A (2002) Coupling HEC-HMS with atmospheric models for prediction of watershed runoff. J Hydrol Eng 7(4):312–318. https://doi.org/10.1061/(ASCE)1084-0699(2002)7:4(312)

Askar MK (2013) Rainfall-runoff model using the SCS-CN method and geographic information systems: a case study of Gomal River watershed. WIT Trans Ecol Environ 4(178):159–170. https://doi.org/10.2495/WS130141

Borga M, Stoffel M, Marchi L, Marra F, Jakob M (2014) Hydrogeomorphic response to extreme rainfall in headwater systems: flash floods and debris flows. J Hydrol 518:194–205. https://doi.org/10.1016/j.jhydrol.2014.05.022

Bougeault P, Lacarrere P (1989) Parameterization of orography-induced turbulence in a mesobeta–scale model. Mon Weather Rev 117(8):1872–1890

Bretherton CS, Park S (2009) A new moist turbulence parameterization in the Community Atmosphere Model. J Clim 22(12):3422–3448

Centre for Research on the Epidemiology of Disasters (2014) The International Disaster Database. EM-DAT

Chatterjee M, De R, Roy D, Das S, Mazumdar A (2014) Hydrological modeling studies with HEC-HMS for damodar basin. India World Appl Sci J 31(12):2148–2154. https://doi.org/10.5829/idosi.wasj.2014.31.12.750

Chen Y, Wen J, Meng X, Zhang Q, Li X, Zhang G, Chen R (2024) An assessment of the coupled weather research and forecasting hydrological model on streamflow simulations over the source region of the Yellow River. Atmosphere (Basel) 15(4):468. https://doi.org/10.3390/atmos15040468

Chou MD, and Suarez MJ (1994) An efficient thermal infrared radiation parameterization for use in general circulation models

Custódio DA, Ghisi E (2023) Impact of residential rainwater harvesting on stormwater runoff. J Environ Manage 326:116814. https://doi.org/10.1016/j.jenvman.2022.116814

Das T, Das S (2024) Event-based flood estimation in un-gauged sub-basins: a comparative assessment of SCS-UH, CWC-UH and Nash-GIUH based rainfall-runoff models in Shilabati River, Eastern India. Nat Hazards 120(15):14153–14178. https://doi.org/10.1007/s11069-024-06765-0

Das T, Das S (2026) An integrated Bayesian hydrodynamic framework for quantifying rating curve uncertainty in design flood estimation and flood hazard mapping in a data-scarce urban area. Water Res 288:124610. https://doi.org/10.1016/j.watres.2025.124610

Deidda R (2000) Rainfall downscaling in a space-time multifractal framework. Water Resour Res 36(7):1779–1794. https://doi.org/10.1029/2000WR900038

Dikici M, Burgan HI (2025) Exploring the effect of meteorological and hydrological trends on groundwater drought index: the case of Seyhan Basin. Ecohydrology. https://doi.org/10.1002/eco.70110

Dudhia J (1989) Numerical study of convection observed during the winter monsoon experiment using a mesoscale two-dimensional model. J Atmos Sci 46(20):3077–3107

Eaton B (2011) User's guide to the Community Atmosphere Model CAM-5.1. NCAR. Cesm. Ucar. Edu/Models/Cesm1. 0/Cam.

Eimanifar A, Mohebbi F (2007) Urmia Lake (Northwest Iran): a brief review. Saline Syst. https://doi.org/10.1186/1746-1448-3-5

Fernández J, Montávez JP, Sáenz J, González-Rouco JF, Zorita E (2007) Sensitivity of the MM5 mesoscale model to physical parameterizations for regional climate studies: annual cycle. J Geophys Res Atmos. https://doi.org/10.1029/2005JD006649

Flesch TK, Reuter GW (2012) WRF model simulation of two Alberta flooding events and the impact of topography. J Hydrometeorol 13(2):695–708. https://doi.org/10.1175/JHM-D-11-035.1

Ghazi B, Dutt S, Torabi Haghighi A (2023) Projection of future meteorological droughts in Lake Urmia Basin, Iran. Water. https://doi.org/10.3390/w15081558

Ghazi B, Salehi H, Cheshami M, Zeydalinejad N, Linh NTT (2025) Projection of climate change impact on main climate variables and assessment of the future of Köppen–Geiger climate classification in Iran. Acta Geophys 73(2):2017–2027. https://doi.org/10.1007/s11600-024-01457-6

Givati A, Gochis D, Rummler T, Kunstmann H (2016) Comparing one-way and two-way coupled hydrometeorological forecasting systems for flood forecasting in the Mediterranean region. Hydrology 3(2):19. https://doi.org/10.3390/hydrology3020019

Goodarzi MR, Pooladi R, Niazkar M (2022a) Evaluation of satellite-based and reanalysis precipitation datasets with gauge-observed data over Haraz-Gharehsoo Basin, Iran. Sustainability 14(20):13051. https://doi.org/10.3390/su142013051

Goodarzi MR, Sabaghzadeh M, Mokhtari MH (2022b) Impacts of aspect on snow characteristics using remote sensing from 2000 to 2020 in Ajichai-Iran. Cold Reg Sci Technol 204:103682. https://doi.org/10.1016/j.coldregions.2022.103682

Goodarzi MR, Poorattar MJ, Vazirian M, Talebi A (2024) Evaluation of a weather forecasting model and HEC-HMS for flood forecasting: case study of Talesh catchment. Appl Water Sci 14(2):34. https://doi.org/10.1007/s13201-023-02079-x

Grell GA, Dévényi D (2002) A generalized approach to parameterizing convection combining ensemble and data assimilation techniques. Geophys Res Lett 29(14):31–38

Grenier H, Bretherton CS (2001) A moist PBL parameterization for large-scale models and its application to subtropical cloud-topped marine boundary layers. Mon Weather Rev 129(3):357–377

Habets F, Lemoigne P, Noilhan J (2004) On the utility of operational precipitation forecasts to served as input for streamflow forecasting. Article J Hydrol. https://doi.org/10.1016/j.hydrol.2004.02.004

Hallegatte S, Green C, Nicholls RJ, Corfee-Morlot J (2013) Future flood losses in major coastal cities. Nat Clim Change 3(9):802–806. https://doi.org/10.1038/nclimate1979

Han J, Pan H-L (2011) Revision of convection and vertical diffusion schemes in the NCEP Global Forecast System. Weather Forecast 26(4):520–533

Hassani A, Azapagic A, D'Odorico P, Keshmiri A, Shokri N (2020) Desiccation crisis of saline lakes: a new decision-support framework for building resilience to climate change. Sci Total Environ 703:134718. https://doi.org/10.1016/j.scitotenv.2019.134718

Hegdahl TJ, Engeland K, Steinsland I, Singleton A (2021) The benefits of pre-and postprocessing streamflow forecasts for an operational flood-forecasting system of 119 Norwegian catchments. Hydrol Earth Syst Sci Discuss 22(2021):1–45. https://doi.org/10.5194/hess-2021-13

Hess P, Boers N (2022) Deep learning for improving numerical weather prediction of heavy rainfall. J Adv Model Earth Syst. https://doi.org/10.1029/2021MS002765

Hong S-Y, Pan H-L (1998) Convective trigger function for a mass-flux cumulus parameterization scheme. Mon Weather Rev 126(10):2599–2620

Hong S-Y, Dudhia J, Chen S-H (2004) A revised approach to ice microphysical processes for the bulk parameterization of clouds and precipitation. Mon Weather Rev 132(1):103–120

Iacono MJ, Delamere JS, Mlawer EJ, Shephard MW, Clough SA, and Collins WD (2008) Radiative forcing by long-lived greenhouse gases: calculations with the AER radiative transfer models. J Geophys Res: Atmos, 113(D13)

Jabbari A, So J-M, Bae D-H (2019) Precipitation forecast contribution assessment in the coupled meteo-hydrological models. Atmosphere (Basel) 11(1):34. https://doi.org/10.3390/atmos11010034

Jahangir MH, Asghari kaleshani F, Ebrahimpour R (2023) Assessment of flooding in future periods using the flow of the watershed (case study: west and south of the Urmia watershed). Nat Hazards Res 3(2):257–270. https://doi.org/10.1016/j.nhres.2023.04.004

Jam-Jalloh SU, Liu J, Wang Y, Liu Y (2024) Coupling WRF with HEC-HMS and WRF-Hydro for flood forecasting in typical mountainous catchments of northern China. Nat Hazards Earth Syst Sci 24(9):3155–3172. https://doi.org/10.5194/nhess-24-3155-2024

Janjić ZI (1994) The step-mountain eta coordinate model: further developments of the convection, viscous sublayer, and turbulence closure schemes. Mon Weather Rev 122(5):927–945

Jansson F, Edeling W, Attema J, Crommelin D (2021) Assessing uncertainties from physical parameters and modelling choices in an atmospheric large eddy simulation model. Philos Trans R Soc A Math Phys Eng Sci 379(2197):rsta.2020.0073. https://doi.org/10.1098/rsta.2020.0073

Jasper K, Kaufmann P (2003) Coupled runoff simulations as validation tools for atmospheric models at the regional scale. Q J R Meteorol Soc 129(588):673–692. https://doi.org/10.1256/qj.02.26

Kain JS (2004) The Kain-Fritsch convective parameterization: an update. J Appl Meteorol 43(1):170–181

Kanji S, Das S (2026) Revealing the relationship between rainfall extremes, atmospheric changes and potential flooding using wavelet and extreme value models. Water Resour Manag. https://doi.org/10.1007/s11269-026-04545-y

Kessler E (1969) On the distribution and continuity of water substance in atmospheric circulations. Springer, pp 1–84

Klemp JB, Dudhia J, Skamarock WC, and Dudhia J (2001) Prototypes for the WRF (Weather Research and Forecasting) model Drought and Flood Monitoring View project PROTOTYPES FOR THE WRF (WEATHER RESEARCH AND FORECASTING) MODEL. https://www.researchgate.net/publication/242446432

Knapp AK, Beier C, Briske DD, Classen AT, Luo Y, Reichstein M, Smith MD, Smith SD, Bell JE, Fay PA, Heisler JL, Leavitt SW, Sherry R, Smith B, Weng E (2008) Consequences of more

extreme precipitation regimes for terrestrial ecosystems. Bioscience 58(9):811–821. https://doi.org/10.1641/B580908
Kumar P, Ojha SP, Singh R, Kishtawal CM, Pal PK (2016) Performance of weather research and forecasting model with variable horizontal resolution. Theor Appl Climatol 126(3–4):705–713. https://doi.org/10.1007/s00704-015-1607-7
Lal M, Mishra SK, Pandey A, Pandey RP, Meena PK, Chaudhary A, Jha RK, Shreevastava AK, Kumar Y (2017) Evaluation of the Soil Conservation Service curve number methodology using data from agricultural plots. Hydrogeol J 25(1):151–167. https://doi.org/10.1007/s10040-016-1460-5
Lim K-SS, Hong S-Y (2010) Development of an effective double-moment cloud microphysics scheme with prognostic cloud condensation nuclei (CCN) for weather and climate models. Mon Weather Rev 138(5):1587–1612
Lin Y, Colle BA (2011) A new bulk microphysical scheme that includes riming intensity and temperature-dependent ice characteristics. Mon Weather Rev 139(3):1013–1035
Lin Y-L, Farley RD, Orville HD (1983) Bulk parameterization of the snow field in a cloud model. J Clim Appl Meteorol 22(6):1065–1092
Lin CA, Wen L, Lu G, Wu Z, Zhang J, Yang Y, Zhu Y, Tong L (2006) Atmospheric-hydrological modeling of severe precipitation and floods in the Huaihe River Basin, China. J Hydrol 330(1–2):249–259. https://doi.org/10.1016/j.jhydrol.2006.03.028
Luo P, Mu D, Xue H, Ngo-Duc T, Dang-Dinh K, Takara K, Nover D, Schladow G (2018) Flood inundation assessment for the Hanoi Central Area, Vietnam under historical and extreme rainfall conditions. Sci Rep 8(1):12623. https://doi.org/10.1038/s41598-018-30024-5
Mahmoudi S, Massah Bavani AR, Ghafarian P (2025) Comparing the outputs of general circulation and mesoscale models in the flood forecasts of mountainous basins. Nat Hazards 121(7):8211–8239. https://doi.org/10.1007/s11069-025-07131-4
Merino A, García-Ortega E, Navarro A, Sánchez JL, Tapiador FJ (2022) WRF hourly evaluation for extreme precipitation events. Atmos Res 274:106215. https://doi.org/10.1016/j.atmosres.2022.106215
Milbrandt JA, Yau MK (2005) A multimoment bulk microphysics parameterization. Part II: a proposed three-moment closure and scheme description. J Atmos Sci 62(9):3065–3081
Monin AS, Obukhov AM (1954) Basic laws of turbulent mixing in the surface layer of the atmosphere. Contrib Geophys Inst Acad Sci USSR 151(163):e187
Najafi MS, Kuchak VS (2024) Ensemble-based monthly to seasonal precipitation forecasting for Iran using a regional weather model. Int J Climatol 44(12):4366–4387. https://doi.org/10.1002/joc.8586
Najafi MS, Sani SAM, Noroozian R, Saribaglou SD (2026) Assessment of C3S monthly to seasonal climate forecast models for mean and extreme precipitation over Iran. Nat Hazards. https://doi.org/10.1007/s11069-025-07786-z
Najafi MS, and Akbari Moghaddam Sani S (2022) Evaluation the performance of three gridded datasets in estimating the time series of extreme precipitation in Iran. Climate Change Res, 3(11), 79–98. https://doi.org/10.30488/ccr.2022.363075.1096
Nakanishi M, Niino H (2004) An improved Mellor-Yamada level-3 model with condensation physics: its design and verification. Bound-Layer Meteorol 112:1–31
Nasiri Z, and Talebi A (2020) Prioritization of sub-basins in terms of flood risk using the HEC-HMS model in the upstream of Shiraz Dry River. Ecohydrology, 7(1), 47–57. https://doi.org/10.22059/ije.2020.284092.1145
Pappenberger F, Cloke HL, Parker DJ, Wetterhall F, Richardson DS, Thielen J (2015) The monetary benefit of early flood warnings in Europe. Environ Sci Policy 51:278–291. https://doi.org/10.1016/j.envsci.2015.04.016
Piadeh F, Behzadian K, Alani AM (2022) A critical review of real-time modelling of flood forecasting in urban drainage systems. J Hydrol 607:127476. https://doi.org/10.1016/j.jhydrol.2022.127476
Pleim JE (2007) A combined local and nonlocal closure model for the atmospheric boundary layer. Part I: model description and testing. J Appl Meteorol Climatol 46(9):1383–1395
Pleim JE, Gilliam R (2009) An indirect data assimilation scheme for deep soil temperature in the Pleim–Xiu land surface model. J Appl Meteorol Climatol 48(7):1362–1376. https://doi.org/10.1175/2009JAMC2053.1
Rogelis MC, Werner M (2018) Streamflow forecasts from WRF precipitation for flood early warning in mountain tropical areas. Hydrol Earth Syst Sci 22(1):853–870. https://doi.org/10.5194/hess-22-853-2018
Rogers E, Black T, Ferrier B, Lin Y, Parrish D, DiMego G (2001) Changes to the NCEP Meso Eta analysis and forecast system: increase in resolution, new cloud microphysics, modified precipitation assimilation, modified 3DVAR analysis. NWS Tech Proced Bull 488:15
Roy D, and Begam S (2013) Calibration and validation of HEC-HMS model for a river basin in eastern India. https://www.researchgate.net/publication/262147296
Shatnawi A, Ibrahim M (2022) Derivation of flood hydrographs using SCS synthetic unit hydrograph technique for Housha catchment area. Water Supply 22(5):4888–4901. https://doi.org/10.2166/ws.2022.169
Shin HH, Hong S-Y (2011) Intercomparison of planetary boundary-layer parametrizations in the WRF model for a single day from CASES-99. Bound-Layer Meteorol 139:261–281
Shrestha DL, Robertson DE, Wang QJ, Pagano TC, Hapuarachchi HAP (2013) Evaluation of numerical weather prediction model precipitation forecasts for short-term streamflow forecasting purpose. Hydrol Earth Syst Sci 17(5):1913–1931. https://doi.org/10.5194/hess-17-1913-2013
Skamarock WC, Klemp JB (2008) A time-split nonhydrostatic atmospheric model for weather research and forecasting applications. J Comput Phys 227(7):3465–3485. https://doi.org/10.1016/j.jcp.2007.01.037
Soleymani k Bashir Gonbad M, Moosavi SR, and Khalighi SH (2006) The potential of flood runoff production in watersheds using the HEC-HMS model in the geographic information system environment, a case study of the Kesilian basin. Natural Geographic Res, 65, 51–60
Soulis KX (2021) Soil Conservation Service Curve Number (SCS-CN) method: current applications, remaining challenges, and future perspectives. Water 13(2):192. https://doi.org/10.3390/w13020192
Sultan D, Tsunekawa A, Tsubo M, Haregeweyn N, Adgo E, Meshesha DT, Fenta AA, Ebabu K, Berihun ML, Setargie TA (2022) Evaluation of lag time and time of concentration estimation methods in small tropical watersheds in Ethiopia. J Hydrol Reg Stud 40:101025. https://doi.org/10.1016/j.ejrh.2022.101025
Tang C, Dennis RL (2014) How reliable is the offline linkage of Weather Research & Forecasting Model (WRF) and Variable Infiltration Capacity (VIC) model? Glob Planet Change 116:1–9. https://doi.org/10.1016/j.gloplacha.2014.01.014
Tedla HZ, Taye EF, Walker DW, Haile AT (2022) Evaluation of WRF model rainfall forecast using citizen science in a data-scarce urban catchment: Addis Ababa, Ethiopia. J Hydrol Reg Stud 44:101273. https://doi.org/10.1016/j.ejrh.2022.101273

Thirel G, Regimbeau F, Martin E, Noilhan J, Habets F (2010) Short- and medium-range hydrological ensemble forecasts over France. Atmos Sci Lett 11(2):72–77. https://doi.org/10.1002/asl.254

Thompson G, Field PR, Rasmussen RM, Hall WD (2008) Explicit forecasts of winter precipitation using an improved bulk microphysics scheme. Part II: implementation of a new snow parameterization. Mon Weather Rev 136(12):5095–5115

Tian J, Liu R, Ding L, Guo L, Liu Q (2021) Evaluation of the WRF physical parameterisations for Typhoon rainstorm simulation in southeast coast of China. Atmos Res 247:105130. https://doi.org/10.1016/j.atmosres.2020.105130

Tiedtke M (1989) A comprehensive mass flux scheme for cumulus parameterization in large-scale models. Mon Weather Rev 117(8):1779–1800

Tunas IG, Azikin H, Oka GM (2021) Impact of extreme rainfall on flood hydrographs. IOP Conf Ser Earth Environ Sci 884(1):012018. https://doi.org/10.1088/1755-1315/884/1/012018

Nations U, and Gov N (n.d.). Guidelines for reducing flood losses national oceanic and atmosphere administration (USA NOAA) www Guidelines for Reducing Flood Losses. Retrieved www.un.org/esa/sustdevwww.unisdr.org

USACE (2000) HEC_HMS Technical manual, hydrologic engineering Center. Davis, CA, 187p

Uwizeyimana D, Mureithi SM, Mvuyekure SM, Karuku G, Kironchi G (2019) Modelling surface runoff using the soil conservation service-curve number method in a drought prone agro-ecological zone in Rwanda. Int Soil Water Conserv Res 7(1):9–17. https://doi.org/10.1016/j.iswcr.2018.12.001

Vargas Garay L, Torres Goyeneche OD, Carrillo Soto GA (2019) Evaluation of SCS - unit hydrograph model to estimate peak flows in watersheds of Norte de Santander. Respuestas 24(1):6–15. https://doi.org/10.22463/0122820x.1743

Vincendon B, Ducrocq V, Dierer S, Kotroni V, Le Lay M, Milelli M, Quesney A, Saulnier G-M, Rabuffetti D, Bouilloud L, Chancibault K, Anquetin S, Lagouvardos K, Steiner P (2009) Flash flood forecasting within the PREVIEW project: value of high-resolution hydrometeorological coupled forecast. Meteorol Atmos Phys 103(1–4):115–125. https://doi.org/10.1007/s00703-008-0315-6

Vincendon B, Ducrocq V, Nuissier O, Vié B (2011) Perturbation of convection-permitting NWP forecasts for flash-flood ensemble forecasting. Nat Hazards Earth Syst Sci 11(5):1529–1544. https://doi.org/10.5194/nhess-11-1529-2011

Weaver JC (2003) Methods for estimating peak discharges and unit hydrographs for streams in the City of Charlotte and Mecklenburg County. North Carolina. https://doi.org/10.3133/wri20034108

Weisman ML, Davis C, Wang W, Manning KW, Klemp JB (2008) Experiences with 0–36-h explicit convective forecasts with the WRF-ARW model. Weather Forecast 23(3):407–437. https://doi.org/10.1175/2007WAF2007005.1

Wild M, Ohmura A, Gilgen H, Morcrette JJ, Slingo A (2001) Evaluation of downward longwave radiation in general circulation models. J Clim 14(15):3227–3239. https://doi.org/10.1175/1520-0442(2001)014%3c3227:EODLRI%3e2.0.CO;2

Yu Z, Lakhtakia MN, Yarnal B, White RA, Miller DA, Frakes B, Barron EJ, Duffy C, Schwartz FW (1999) Simulating the river-basin response to atmospheric forcing by linking a mesoscale meteorological model and hydrologic model system. J Hydrol 218(1–2):72–91. https://doi.org/10.1016/S0022-1694(99)00022-0

Zhang C, Wang Y, Hamilton K (2011) Improved representation of boundary layer clouds over the Southeast Pacific in ARW-WRF using a modified Tiedtke cumulus parameterization scheme*. Mon Weather Rev 139(11):3489–3513. https://doi.org/10.1175/MWR-D-10-05091.1

Zhang T, Gao Y, Yu P, Li J, Feng P, and Ma HX (2023) Improving flood forecasts capability of Taihang Piedmont basin by coupling WRF and HEC-HMS. https://doi.org/10.21203/rs.3.rs-3139605/v1

Zhou J, Zhang H, Zhang J, Zeng X, Ye L, Liu Y, Tayyab M, Chen Y (2018) WRF model for precipitation simulation and its application in real-time flood forecasting in the Jinshajiang River Basin, China. Meteorol Atmos Phys 130(6):635–647. https://doi.org/10.1007/s00703-017-0542-9

Ziegler CL (1985) Retrieval of thermal and microphysical variables in observed convective storms. Part 1: model development and preliminary testing. J Atmos Sci 42(14):1487–1509

Publisher's Note Springer Nature remains neutral with regard to jurisdictional claims in published maps and institutional affiliations.